DE GRUYTER OPEN

Eur. Pharm. J. 2017, 64 (2): 1-3.
ISSN 1338-6786 (online) and ISSN 2453-6725 (print version),
DOI: 10.1515/afpuc-2017-0012

EUROPEAN PHARMACEUTICAL JOURNAL

Partial molecular volumes of cholesterol and phosphatidylcholine in mixed bilayers

Original Paper

Gallová J.✉, Želinská K., Balgavý P.

Comenius University in Bratislava, Faculty of Pharmacy, Department of Physical Chemistry of Drugs, Bratislava, Slovak Republic

Received 22 June, 2016, accepted 19 July, 2016

Abstract Dispersion of multilamellar liposomes of dimyristoylphosphatidylcholine (DMPC) and cholesterol (CHOL) were studied by vibrational densitometer for the CHOL mole fractions $X = 0–0.54$ in the temperature range 18–50 °C, both below and above the main phase transition. DMPC-CHOL bilayers served as a simple model for lipidic part of biological membrane. Volumetric parameters are essential not only to evaluate the data obtained by scattering and diffraction methods on model membranes but can provide valuable information about molecular packing in bilayers and the phase behaviour of lipid-CHOL mixtures. In this paper, preliminary results regarding the changes in the specific volume of lipid bilayer with increasing temperature and CHOL content are presented. Different values of apparent molecular volume of CHOL for different CHOL mole fraction pointed out the non-ideal mixing of DMPC and CHOL.

Keywords – *cholesterol, dimyristoylphosphatidylcholine, specific volume, densitometry*

INTRODUCTION

In biological systems, CHOL is known to play a fundamental role as a modulator of physical properties and lateral organization of the membrane lipid bilayer. Thus, many studies of the interaction of CHOL with phospholipid bilayer model membranes have been performed, utilizing a wide range of physical techniques (for a review, see Marquardt et al., 2016). In our recent paper (Gallová et al., 2015), we determined the molecular volumes of CHOL and of a series of monounsaturated diacylphosphatidylcholines with the number of carbon atoms in the acyl chain 16, 18, 20, 22 and 24 in the temperature range 20–40 °C in mixed bilayer. This work is devoted to the preliminary study of volumetric parameters of DMPC and CHOL in mixed bilayers. The knowledge of these parameters is essential to evaluate the data obtained by scattering and diffraction methods on model membranes. Greenwood et al. (2006) studied the binary systems of CHOL with different phospholipids at limited temperature points. In this paper, changes in volumetric parameters of CHOL and DMPC in mixed bilayers induced by increasing temperature and CHOL content are studied.

MATERIAL AND METHODS

Chemicals: 1,2-dimyristoyl-*sn*-glycero-3-phosphocholine (DMPC) was purchased from Avanti Polar Lipids (Alabaster, Alabama), CHOL from Sigma Aldrich (Germany) and chloroform, p.a. from Slavus (Bratislava, Slovakia).

Sample preparation: DMPC and CHOL were weighed in a dry state into a glass vial and then co-dissolved with a small amount of chloroform. The solution was mixed thoroughly. The solvent was evaporated to dryness under a stream of gaseous nitrogen, followed by evacuation in a vacuum chamber. The dry lipid film was hydrated by the weighed amounts of deionised water to obtain the final concentration of lipid ≈1–3 % (w/w). Multilamellar liposomes were formed during vortexing and brief sonication in a bath sonicator. Samples were heated to 30 °C and degassed before measurement. The density of prepared samples and also of deionised water was measured using vibrational densitometer DMA 4500M (Anton Paar, Austria) in the temperature range 16–50 °C with step 1 °C. Weighing errors were ± 0.0001 g; the precision of the density measurement was ± 0.00005 g/cm^3.

* *E-mail: gallova@fpharm.uniba.sk*

Data treatment: The specific volume of the sample, v_S, is a reciprocal value of the sample density measured by a densitometer. According to (Greenwood et al., 2006; Klacsová et al., 2010) we assumed that the specific volume of water in our samples is the same as in pure bulk water. Under this precondition, the apparent specific volume of DMPC, v_{PC}, was calculated from the specific volume of the control sample v_{S0} without cholesterol, according to the equation 1

$$v_{PC} = \frac{v_{S0} - (1 - w_{PC})v_W}{w_{PC}} \quad (1)$$

where, v_W is the specific volume of water and w_{PC} is the mass fraction of DMPC in the control sample defined as

$$w_{PC} = \frac{m_{PC}}{m_{PC} + m_W} \quad (2)$$

where, m_{PC} and m_W are masses of DMPC and water in the sample, respectively. The apparent specific volume of the nonaqueous part (DMPC + cholesterol) of the sample, v_{PC+CH}, was calculated in a similar way:

$$v_{PC+CH} = \frac{v_S - (1 - w_{PC+CH})v_W}{w_{PC+CH}} \quad (3)$$

where, w_{PC+CH} is the mass fraction of lipid part in the sample defined as

$$w_{PC+CH} = \frac{m_{PC} + m_{CH}}{m_{PC} + m_{CH} + m_W} \quad (4)$$

If we further suppose that the specific volume of DMPC in the sample does not depend on the CHOL content, the apparent specific volume of CHOL, v_{CH}, can be calculated using the equation:

$$v_{CH} = \frac{v_{PC+CH} - (1 - w_{CH})v_{PC}}{w_{CH}} \quad (5)$$

where, w_{CH} is the mass fraction of CHOL in the lipidic part of the sample defined as

$$w_{CH} = \frac{m_{CH}}{m_{PC} + m_{CH}} \quad (6)$$

where, m_{CH} is the mass of CHOL in the sample. The apparent specific volume of CHOL was converted to the apparent molecular volume V_{CH} using the following relation:

$$V_{CH} = \frac{v_{CH} M_{CH}}{N_A} \quad (7)$$

where, M_{CH} is the molar mass of CHOL and N_A is the Avogadro's number.

RESULTS AND DISCUSSION

The density of samples containing multilamellar liposomes of DMPC and CHOL was measured in the temperature range 16–50 °C. The apparent specific volume of the lipid (nonaqueous) part of samples was calculated for the control sample without CHOL, v_{PC}, and for samples containing CHOL, v_{PC+CH}, according to equations 1–4. Because the partial molecular volume of water located in bilayers is the same as the molecular volume in the bulk water (for references, see Uhríková et al., 2007), the expression 'apparent' is omitted and the fully hydrated lipid bilayers in multilamellar liposomes were treated as a separate phase. As expected, the specific volume v_{PC+CH} increases with increasing temperature for various mole fractions of CHOL (Fig. 1).

It is well known that the hydrated bilayers of DMPC are in a solid-ordered S_o phase at $t<t_p$ (temperature of pretransition), in a rippled $P_ß$ phase at $t_p<t<t_m$ and in a disordered fluid phase L_d above the main phase transition temperature t_m. The main phase transition is clearly visible from the temperature dependence of v_{PC} (CHOL-free DMPC bilayers). According to McMullen and et al. (1993), a small amount of CHOL is able to abolish the pretransition in DMPC bilayers. In this work, the pretransition was not included in the measured temperature

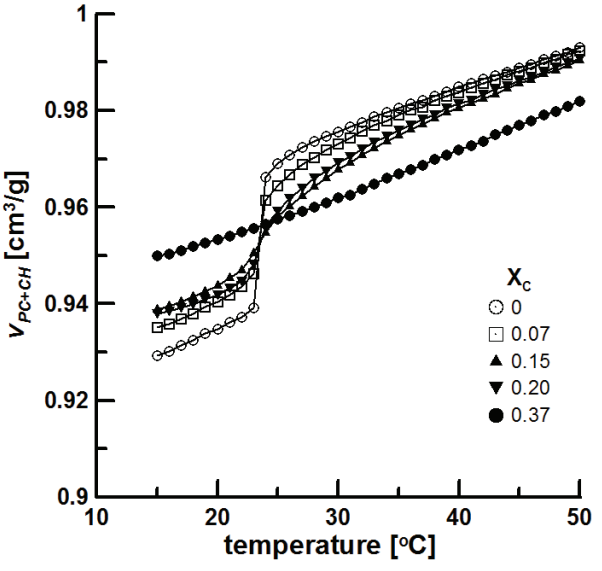

Figure 1. Temperature dependence of the specific volume of DMPC-CHOL bilayers with varying content of CHOL. Numbers denote mole fraction of CHOL

range and all the samples were heated above t_m just before the measurement to avoid a rippled $P_ß$ phase formation. The observed main phase transition temperature t_m = 23–24 °C in the control DMPC sample is in agreement with data from the literature (McMullen and et al., 1993). The values of DMPC specific volume are similar to the data of Nagle & Wilkinson (1978). The main phase transition at low CHOL mole fractions ($X < 0.1$) was narrow and only a small decrease of t_m (within the temperature range of 1 °C) was observed (Fig. 1).

The transition was broadened around $X = 0.1$ and was not detectable at $X \geq 0.3$ (Fig. 1). These observations are similar to those in McMullen et al. (1993). It is widely accepted that cholesterol can induce a liquid-ordered L_o state in lipid membranes containing high amount of cholesterol. L_o state was described by Vist & Davis (1990) as a phase with properties intermediate between S_o and L_d phases. The L_o phase is stable in a wide temperature range. We can therefore suppose that the samples with high CHOL content, where the main phase transition is not visible (Fig. 1), contain DMPC-CHOL bilayers in liquid-ordered L_o state.

The apparent specific volume of CHOL, v_{CH}, was calculated (eq. 5,6) and converted further to the apparent molecular volume of CHOL, V_{CH} (eq. 7). As seen from the Fig. 2, V_{CH} changes when the mole fraction X of CHOL increases, especially at low X. Our preliminary results confirm the fact that CHOL and DMPC do not mix ideally.

In conclusion, we have determined the temperature dependence of specific volume of DMPC bilayers with various amount of CHOL and the temperature dependence of apparent molecular volume of CHOL in the mixed DMPC-CHOL bilayers. We have confirmed a non-ideal mixing of CHOL and DMPC. The paper, where the partial molecular volumes of CHOL and DMPC will be calculated in dependence on temperature and CHOL content, is being in preparation.

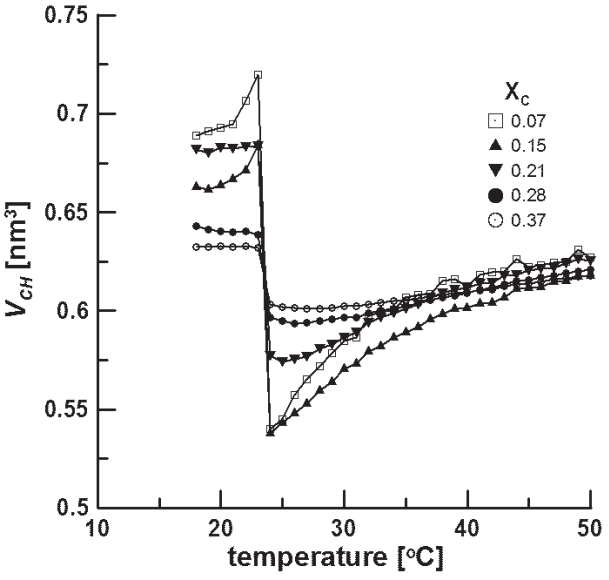

Figure 2. Temperature dependence of the apparent molecular volume of CHOL in DMPC-CHOL bilayers with varying contents of CHOL. Numbers denote mole fraction of CHOL

ACKNOWLEDGEMENT

This work was supported by the Dubna JINR project 04-4-1121-2015/2017 and by the VEGA grant 1/0916/16 and 1/0228/17.

References

[1] Gallová J, Klacsová M, Devínsky F, Balgavý P. Partial volumes of cholesterol and monounsaturated diacylphosphatidylcholines in mixed bilayers. Chem. Phys. Lipids 2015;190:1-8.

[2] Greenwood AI, Tristram-Nagle S, Nagle JF. Partial molecular volumes of lipids and cholesterol. Chem. Phys. Lipids 2006;143:1-10.

[3] Klacsová M, Westh P, Balgavý P. Molecular and component volumes of saturated n-alkanols in DOPC plus DOPS bilayers. Chem. Phys. Lipids 2010;163:498-505.

[4] Marquardt D, Kučerka N, Wassall SR, Harroun TA, Katsaras J. Cholesterol's location in lipid bilayers. Chem. Phys. Lipids 2016;199:17-25.

[5] McMullen TP, Lewis RN, McElhaney RN. Differential scanning calorimetric study of the effect of cholesterol on the thermotropic phase behavior of a homologous series of linear saturated phosphatidylcholines. Biochemistry 1993;32:516-522.

[6] Nagle JF, Wilkinson DA. Lecithin bilayers. Density measurement and molecular interactions. Biophys. J. 1978;23:159-175.

[7] Uhríková D, Rybár P, Hianik T, Balgavý P. Component volumes of unsaturated phosphatidylcholines in fluid bilayers: a densitometric study. Chem. Phys. Lipids 2007;145:97-105.

[8] Vist MR, Davis JH. Phase equilibria of cholesterol/dipalmitoylphosphatidylcholine mixtures: ^{2}H nuclear magnetic resonance and differential scanning calorimetry. Biochemistry 1988;29:451-464.

DE GRUYTER OPEN

Eur. Pharm. J. 2017, 64 (2): 4-8.
ISSN 1338-6786 (online) and ISSN 2453-6725 (print version),
DOI: 10.1515/afpuc-2017-0010

EUROPEAN PHARMACEUTICAL JOURNAL

Effect of alkan-1-ols on the structure of dopc model membrane

Original Paper

Kondela T.[1]✉, Gallová J.[1], Hauß T.[2], Ivankov O.[3,4,5], Kučerka N.[1,3], Balgavý P.[1]

[1]Comenius University in Bratislava, Faculty of Pharmacy, Department of Physical Chemistry, Bratislava, Slovak Republic
[2]Helmholtz Zentrum Berlin für Materialen und Energie, Berlin, Germany
[3]Frank Laboratory of Neutron Physics, Joint Institute for Nuclear Research, Dubna, Russia
[4]Moscow Institute of Physics and Technology, MIPT, Dolgoprudny, Russia
[5]Institute for Safety Problems of Nuclear Power Plants, NAS Ukraine, Kiev, Ukraine

Received 20 June, 2017, accepted 6 July, 2017

Abstract The effect of general anaesthetics alkan-1-ols (CnOH, where n = 10, 12, 14, 16 and 18 is the number of carbon atoms in the molecule) on the structure of dioleoylphosphatidylcholine (DOPC) model membrane was studied by small-angle neutron scattering (SANS) and small-angle neutron diffraction (SAND). Fluid bilayers were prepared at CnOH:DOPC = 0.3 molar ratio. The results of both the experiments show that bilayer thickness – a thickness parameter d_g in the case of SANS and lamellar repeat distance D in the case of SAND – increases with increasing n. A coexistence of two lamellar phases with different D was detected by measuring the C18OH+DOPC oriented sample.

Keywords *Model membrane – general anaesthetics – alkan-1-ols – small-angle neutron scattering – small-angle neutron diffraction – structure*

INTRODUCTION

Long-chain primary alcohols (alkan-1-ol or CnOH, where n is the number of carbons in aliphatic chain) display several biological activities (Fujita et al., 2008; Kubo et al., 1995; Pringle et al., 1981). The most widely known are their general anaesthetic properties (Pringle et al., 1981), which are believed to result from their interactions with biological membranes. Whilst the origin of the anaesthetic effect is discussed in terms of both their specific interactions with membrane proteins or via structural changes in lipid bilayers, neither mechanism is described adequately. Because of their amphiphilic structure, CnOHs penetrate into lipid bilayers of biomembranes and change their structural and dynamic properties. Some of these changes may be related to biological effects of CnOHs. Their anaesthetic potency increases with the increase in n up to n = 11 and then decreases. The compounds with n > 13 are non-anaesthetic (Pringle et al., 1981). Such dependence on the chain length is typical for different types of biological activities of homologous series of amphiphilic molecules with long-chain substituents and is called the cut-off effect. The lipid theory of cut-off effect supposes that amphiphiles influence physical properties of lipid bilayers, for example, the bilayer thickness, and thereby induce conformational changes in transmembrane proteins, resulting in the blockage of ion channels (Balgavý & Devínsky, 1996). In this contribution, we study the effects of CnOH (n = 8–18) on a model membrane, the dioleoylphosphatidylcholine (DOPC) bilayers, which resemble the lipid part of biological membrane. Preliminary results obtained from experiments performed by small-angle neutron diffraction (SAND) and small-angle neutron scattering (SANS) are presented.

MATERIALS AND METHOD

DOPC was purchased from Avanti Polar Lipids (Alabaster, USA), saturated and unbranched CnOHs (n = 10, 12, 14, 16, 18) were from Sigma-Aldrich (St. Louis, USA) and heavy water (99.98% D_2O) was from Izotop (Moscow, Russia) and Chemotrade (Leipzig, Germany). Spectrosil 2000 quartz plates (75 mm × 25 mm) were from Saint-Gobain Quartz (Saint-Gobain, France). Oriented samples were prepared for SAND measurements. Calculated amounts of DOPC and CnOH were co-dissolved in chloroform–methanol mixture (3:1 v/v) in glass vials to

* E-mail: kondela@fpharm.uniba.sk

achieve CnOH:DOPC molar ratio of 0.3. Approximately 20 mg of DOPC or DOPC + CnOH in solution were spread onto a 75 cm × 25 cm quartz glass and rocked during evaporation of organic solvent (Tristram-Nagle, 2007). The remaining traces of solvent were evaporated by vacuum pump, which was done at reduced temperature (–10 °C) to avoid the loss of volatile CnOHs. Before each measurement, samples were equilibrated for 24 h at 98% relative humidity (RH) and temperature of 25 °C. The samples were hydrated from a vapour phase over saturated K_2SO_4 solution at three different D_2O/H_2O contrasts (8%, 20% and 50% of D_2O) to determine the phases of structure factors for the Fourier transformation. Measurements were performed using the neutron Membrane Diffractometer V1 equipped by a ^{3}He position-sensitive detector at the BER II reactor of the Helmholtz-Zentrum Berlin für Materialien und Energie. Neutron wavelength was selected at λ = 4.5707 Å.

Dispersions of unilamellar liposomes were prepared for SANS measurements. Calculated amounts of DOPC and CnOH were co-dissolved in chloroform–methanol mixture (3:1 v/v) in glass vials to achieve CnOH:DOPC molar ratio of 0.3. Lipid was dried by a stream of gaseous nitrogen. The rest of the solvent was removed by vacuum pump. Lipid film was hydrated by 100% D_2O so that the weight percentage of DOPC + CnOH in D_2O was less than 2%. The dispersion of multilamellar liposomes arising in the process of agitation was then extruded through a polycarbonate membrane filter with 50-nm diameter pores. The extrusion technique is suitable to produce unilamellar liposomes with a reasonably homogeneous diameter distribution (polydispersity of about 30%) with a mean diameter approaching the polycarbonate membrane pore diameter (Kucerka et al., 2007). The samples of unilamellar liposomes dispersion were poured into 1-mm thick quartz cells and measured at 25.0 ± 0.1 °C. The SANS measurements were performed at the time-of-flight spectrometer YuMO with two-detector system at IBR-2 fast pulse reactor of Frank Laboratory of Neutron Physics in Joint Institute for Nuclear Research in Dubna, Russia (Kuklin et al., 2012). The scattering curves were corrected for background (Soloviev et al., 2003).

RESULTS AND DISCUSSION

We study the interaction of homologous series of alkan-1-ols with a model membrane represented by DOPC bilayers. Fully hydrated DOPC lipids form a fluid lamellar phase at temperatures above –17 °C (Lewis et al., 1988). Because of their amphiphilic structure, alcohols (CnOH, n = 8–18) are intercalated in DOPC bilayer with their hydroxyl groups in the head-group region of DOPC and the hydrophobic chains parallel to the acyl chains of DOPC. It was found that DOPC + CnOHs (n = 8–18) also form homogeneous fluid bilayers without phase separation at least to CnOH:DOPC molar ratio of 0.4 (Kotalová et al., 2008).

In oriented samples, bilayers of CnOH + DOPC are aligned parallel to the flat surface of the quartz plate. Individual lipid bilayers are separated by layers of water. The number of water molecules per one DOPC molecule is only approaching the condition of full hydration because samples were hydrated in the surroundings with 98% RH. Such partial dehydration was, however, shown not to affect, for the most part, the bilayer structural parameters (Kucerka et al., 2009). A regular arrangement of lipid bilayers separated by interlamellar water layers causes a diffraction of neutron beam applied at small scattering angle θ (angle between the incident neutron beam and the planar surface of the bilayer). Typical diffractogram contained five to seven diffraction peaks. As an example, diffractogram obtained by C10OH + DOPC oriented sample is shown in Fig. 1.

Diffraction peaks were fitted to Gaussians sitting atop of linear function describing the background. The equal distance between maxima of individual diffraction peaks confirms the lamellar arrangement. The position of peaks is given by the Bragg law,

$$h\lambda = 2D \sin(\theta), \quad (1)$$

where h is the order of diffraction peak, λ is the wavelength of neutrons and D is the minimum distance between periodically repeated structures. The repeat distance D is the sum of the thickness of the lipid bilayer D_B and the thickness of the water layer D_W ($D = D_B + D_W$). The dependence of the repeat distance D on the chain length of CnOH is shown in Fig. 2. It is clearly seen that shorter alcohols (n = 10–14) cause a decrease in D in DOPC multilayers where C10OH is the most effective. Longer alcohol, C16OH, increases the repeat distance. Two lamellar phases with different repeat spacing were detected in the sample containing C18OH (see inset to Fig. 1). C18OH and DOPC probably do not mix ideally at the molar ratio of 0.3 and level of hydration used, and two phases with different C18OH:DOPC molar ratio are created. Similar diffractograms were obtained after repeated preparation of C18OH + DOPC oriented sample.

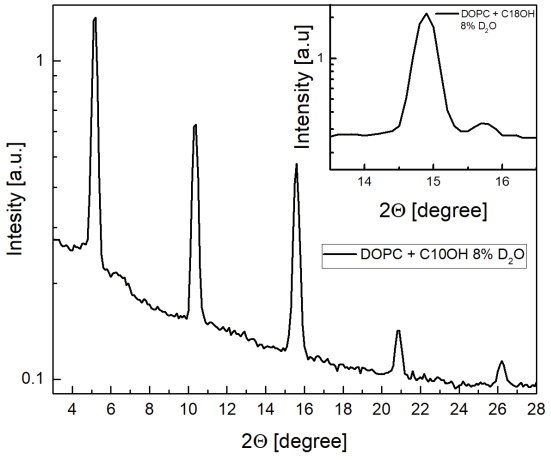

Figure1. Diffractogram of oriented C10OH + DOPC multilayers hydrated at 98% RH and D2O/H2O contrast of 8%. Inset – the third peak in the diffractogram of DOPC + C18OH multilayers documenting phase superposition.

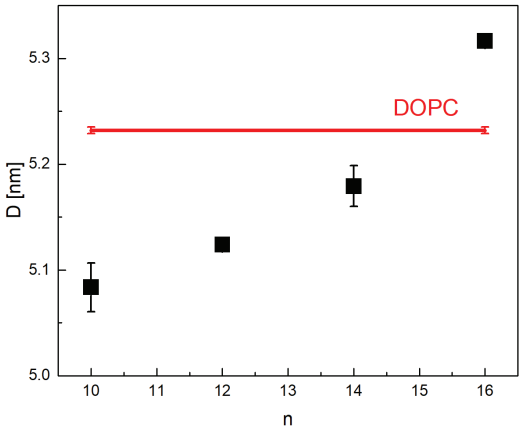

Figure2. Dependence of the repeat distance D on CnOH alkyl length n. Horizontal line – DOPC as a reference.

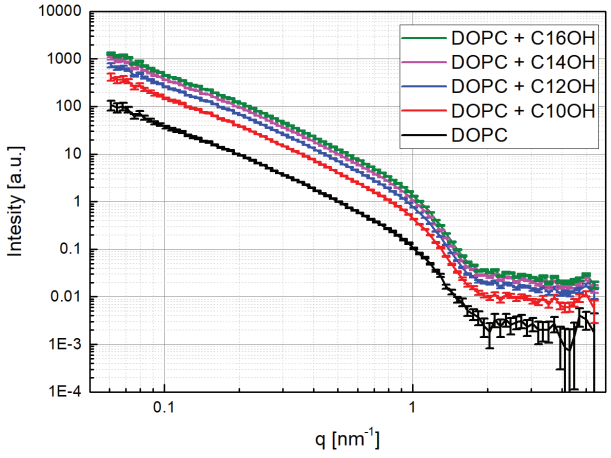

Figure3. Experimental SANS data obtained from unilamellar liposomes of DOPC + CnOH dispersed in D_2O. Scattering curves are shifted vertically for clarity of presentation. From bottom to top, they correspond to DOPC bilayers and DOPC containing C10OH, C12OH, C14OH and C16OH, respectively.

Results obtained with C18OH + DOPC, though a relative amount of the secondary phase can be estimated to be less than 5%, are, therefore, excluded from further data analysis.

A similar study was performed with non-oriented samples at full hydration (Petrenko et al., 2010). The increase in D with increasing n in CnOH:DOPC bilayer was also observed. Because of full hydration, the values of D were higher (6.03 nm for pure DOPC) and characteristic of the higher experimental error. Figure 2 shows that CnOH (n = 10–16) are able to influence the repeat distance D of DOPC-stacked bilayers at CnOH:DOPC molar ratio of 0.3. On the presented level of evaluation, it is not possible to distinguish whether D_B or D_W or both of them are influenced by CnOH. SAND patterns measured at various D_2O/H_2O contrasts also include information regarding the internal structure of the lipid bilayer. After the correction of Bragg peak intensities for incident flux, sample absorption and Lorentz correction, form factor phases can be determined through the isotopic replacement of H_2O for D_2O. Scattering length density profile of the bilayer can then be acquired using scattering form factors through their Fourier transformation. This more advanced evaluation described, for example, in Kucerka et al., 2009 will be presented in future.

Experimental SANS data are dependencies of scattered intensity I on the scattering vector modulus $q = 4\pi\sin(\theta)/\lambda$. Scattering curves for DOPC and CnOH + DOPC are shown in Fig. 3. It was experimentally shown (see, e.g. Kučerka et al., 2003, for citations) that the interparticle interaction between unilamellar liposomes is negligible at the lipid concentrations and liposome sizes used. When the bilayer thickness is small compared to liposome radii, neutron scattering on liposomes can be approximated by the scattering on randomly oriented planar sheets having the same thickness d_g. The Kratky–Porod approximation can be used in some range of q:

$$I(q)=Aq^{-2}\exp(-q^2R_g^2), \quad (2)$$

where A is a scaling constant and R_g is the radius of gyration. The thickness of two-dimensional planar sheet d_g ($d_g^2=12R_g^2$) can be determined using the Kratky–Porod plot ($\mathrm{Ln}(Iq^2)=f(q^2)$). We found that d_g = 3.93 ± 0.08 nm for DOPC without CnOH similar to 3.78 ± 0.02 nm (Kučerka et al., 2003), 3.90 ± 0.08 nm (Uhríková et al., 2000), 3.92 ± 0.06 nm (Uhríková et al., 2003) and 3.91 ± 0.02 nm (Uhríková et al., 2001).

It was shown that bilayer thickness parameter d_g is linearly correlated with the transbilayer phosphate–phosphate distance in unilamellar diacylphosphatidylcholine liposomes (Balgavý et al., 2001). This indicates that changes in thickness parameter d_g can reflect rather well changes in the bilayer thickness. Obviously, the values of d_g are smaller than the steric thickness (e.g. 4.97 ± 0.07 nm for pure DOPC; Kučerka et al., 2007) obtained when taking into account the internal structure of the bilayer with some water molecules penetrating into the polar region of the bilayer. Figure 4 shows that the bilayer thickness parameter d_g increases with increasing n reaching the d_g value of pure DOPC bilayer at C16OH. However, the decrease in d_g caused by the shortest alcohol C10OH is only mild, around 0.1 nm. Unfortunately, the experimental error of d_g is quite large. We suppose that more precise values of the bilayer thickness will be obtained by fitting of the scattering curve in a broader range of q in advanced evaluation using a more realistic model of SANS on unilamellar vesicles as shown in our previous papers (e.g. Gallová et al., 2011).

Similar effect of CnOH on the lipid bilayer thickness as shown in Fig. 4 was observed in Klacsová et al. (2011), wherein the steric thickness of the mixed DOPC–DOPS (dioleoylphosphatidylserine) bilayer (DOPC:DOPS molar ratio of ~25) was studied by SANS. The decrease in the bilayer thickness caused by short alcohols was explained by the mismatch between the chain length of CnOH and lipid– the insertion of shorter alcohol molecule into a lipid bilayer creates a free space under its terminal methyl group, which is filled-in

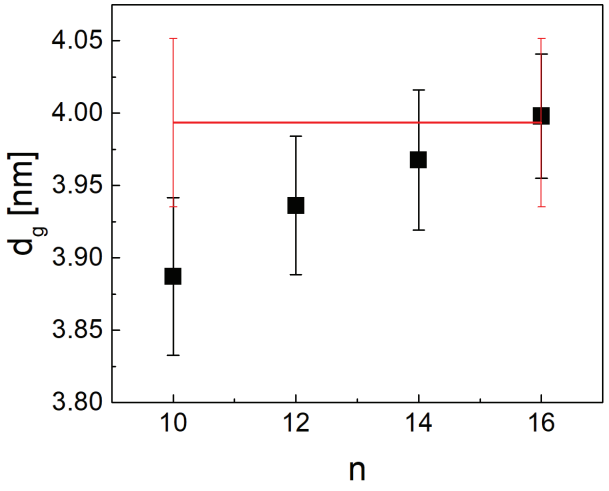

Figure4. Dependence of the bilayer thickness parameter dg on CnOH alkyl length n. Horizontal line – DOPC as a reference.

with neighbouring lipid acyl chains. This causes a decrease in the bilayer thickness. Such defects become smaller when longer-chain alcohol is intercalated in the same bilayer.

In conclusion, the preliminary results of SAND experiments on aligned planar bilayers with limited hydration show that shorter alcohols (CnOH, n = 10–14) decrease the repeat distance, whilst C16OH causes its increase. It was determined using SANS that the parameter of the bilayer thickness d_g increases with increasing n reaching the d_g value of pure DOPC bilayer at C16OH.

ACKNOWLEDGEMENT

This work was supported by VEGA grants 1/0916/16, 1/0228/17, Dubna JINR 04-4-1121-2015/2017 project and European Commission under the 7th Framework Programme through the 'Research Infrastructure' action of the 'Capacities' Programme, NMI3-II Grant number 283883. We thank the HZB and JINR for providing the neutron beam time with the accepted proposals.

References

[1] Balgavý P, Devínsky F. Cut-off effects in biological activities of surfactants. Adv Colloid Interfac. 1996;66:23–63.

[2] Balgavý P, Dubničková M, Kučerka N, Kiselev MA, Yaradaikin SP, Uhríková D. Bilayer thickness and lipid interface area in unilamellar extruded 1,2-diacylphosphatidylcholine liposomes: A small-angle neutron scattering study. Biochim Biophys Acta. 2001;1512:40–52.

[3] Fujita KI, Fujita T, Kubo I. Antifungal activity of alkanols against Zygosaccharomyces bailii and their effects on fungal plasma membrane. Phytother Res. 2008;22:1349–55.

[4] Gallová J, Uhríková D, Kučerka N, Svorková M, Funari SS, Murugova TN, Balgavý P. Influence of cholesterol and β-sitosterol on the structure of EYPC bilayers. J Membr Biol. 2011;243:1.

[5] Hope MJ, Bally MB, Mayer LD, Janoff AS, Cullis PR. Generation of multilamellar and unilamellar phospholipid vesicles. Chem Phys Lipids. 1986;40:89–107.

[6] Hope MJ, Bally MB, Webb G, Cullis PR. Production of large unilamellar vesicles by a rapid extrusion procedure. Characterization of size distribution, trapped volume and ability to maintain a membrane potential. Biochim Biophys Acta. 1985;812:55–65.

[7] Klacsová M, Bulacu M, Kučerka N, Uhríková D, Teixeira J, Marrink SJ, Balgavý P. The effect of aliphatic alcohols on fluid bilayers in unilamellar DOPC vesicles--a small-angle neutron scattering and molecular dynamics study. Biochim Biophys Acta. 2011;1808:2136–46.

[8] Kotalová M, Uhríková D, Funari SS, Balgavý P. Influence of long-chain alcohols on structural parameters of DOPC bilayers. In: HASYLAB Annual Report 2007. 2008; Hamburg.

[9] Kubo I, Muroi H, Kubo A. Structural functions of antimicrobial long-chain alcohols and phenols. Bioorg Med Chem. 1995;3:873–880.

[10] Kucerka N, Nieh M, Pencer J, Sachs J, Katsaras J. What determines the thickness of a biological membrane. Gen Physiol Biophys. 2009;28:117–125.

[11] Kučerka N, Uhríková D, Teixeira J, Balgavý P. Lipid Bilayer Thickness In Extruded Liposomes Prepared From 1 , 2-Diacylphosphatidylcholines With Monounsaturated Acyl Chains : A Small-Angle Neutron Scattering Study. Acta Fac Pharm Univ Comen. 2003;50:78–89.

[12] Kučerka N, Pencer J, Nieh MP, Katsaras J. Influence of cholesterol on the bilayer properties of monounsaturated phosphatidylcholine unilamellar vesicles. Eur Phys J E. 2007;23:247–254.

[13] Lewis RNAH, Sykes BD, McElhaney RN. Thermotropic phase behavior of model membranes composed of phosphatidylcholines containing cis-monounsaturated acyl chain homologs of oleic acid: differential scanning calorimetric and phosphorus-31 NMR spectroscopic studies. Biochemistry. 1988;27:880–887

[14] Mayer LD, Hope MJ, Cullis PR. Vesicles of variable sizes produced by a rapid extrusion procedure. Biochim Biophys Acta. 1986;858:161–168.

[15] Olson F, Hunt CA, Szoka FC, Vail WJ, Papahadjopoulos D. Preparation of liposomes of defined size distribution by extrusion through polycarbonate membranes. Biochim Biophys Acta. 1979;557:9–23.

[16] Petrenko VI, Klacsova M, Beskrovnyy AI, Uhrikova D, Balgavy P. Interaction of long-chain n-alcohols with fluid DOPC bilayers: a neutron diffraction study. Gen Physiol Biophys. 2010;29:355–61.

[17] Pringle MJ, Brown K B, Miller KW. Can the lipid theories of anesthesia account for the cutoff in anesthetic potency in homologous series of alcohols? Mol Pharmacol. 1981;19:49–55.

[18] Soloviev AG, Solovieva TM, Stadnik AV, Islamov AK, Kuklin AI. SAS. Program for primary processing of small-angle scattering spectra. Version 2.4. Description and user guide. Soobshch Ob\cdprime ed Inst Yadernykh Issled Dubna. 2003;P10-2003-86.

[19] Tristram-Nagle SA. Preparation of oriented, fully hydrated lipid samples for structure determination using X-ray scattering. Methods Mol Biol. 2007;400:63–75.

[20] Uhríková D, Balgavý P, Kučerka N, Islamov A, Gordeliy V, Kuklin A. Small-angle neutron scattering study of the n-decane effect on the bilayer thickness in extruded unilamellar dioleoylphosphatidylcholine liposomes. Biophys Chem. 2000;88:165–170.

[21] Uhríková D, Kučerka N, Islamov A, Gordeliy V, Balgavý P. Small-angle neutron scattering study of N-dodecyl-N,N-dimethylamine-N-oxide induced solubilization of dioleoylphosphatidylcholine bilayers in liposomes. Gen. Physiol. Biophys. 2001;20:183–189.

[22] Uhríková D, Kučerka N, Islamov A, Kuklin A, Gordeliy V, Balgavý P. Small-angle neutron scattering study of the lipid bilayer thickness in unilamellar dioleoylphosphatidylcholine vesicles prepared by the cholate dilution method: n-decane effect. Biochim Biophys Acta. 2003;1611:31–34.

DE GRUYTER OPEN

Eur. Pharm. J. 2017, 64 (2): 9-14.
ISSN 1338-6786 (online) and ISSN 2453-6725 (print version),
DOI: 10.1515/afpuc-2016-0018

EUROPEAN PHARMACEUTICAL JOURNAL

Cation-containing lipid membranes – experiment and md simulations

Original Paper

Kučerka N.,[1,2]✉ Dushanov E.,[3] Kholmurodov KT.,[2,4] Katsaras J.,[5-7] and Uhríková D.[1]

[1]Comenius University in Bratislava, Faculty of Pharmacy, Department of Physical Chemistry of Drugs, Bratislava, Slovak Republic
[2]Frank Laboratory of Neutron Physics, [3]Joint Institute for Nuclear Research, Laboratory of Radiation Biology, Dubna - Moscow Region, Russia
[4]Dubna State University, Dubna Moscow Region, Russia
[5]Oak Ridge National Laboratory, Shull Wollan Center: A Joint Institute for Neutron Sciences, Oak Ridge, Tennessee 37831, United States
[6]Oak Ridge National Laboratory, Biology and Soft Matter Division, Oak Ridge, Tennessee 37831, United States
[7]University of Tennessee, Department of Physics and Astronomy, United States

Received 15 September, 2016, accepted 7 November, 2016

Abstract Using small angle neutron diffraction and molecular dynamics simulations we studied the interactions between calcium (Ca^{2+}) or zinc (Zn^{2+}) cations, and oriented gel phase dipalmitoyl-phosphatidylcholine (DPPC) bilayers. For both cations studied at ~1:7 divalent metal ion to lipid molar ratio (Me^{2+}:DPPC), bilayer thickness increased. Simulation results helped reveal subtle differences in the effects of the two cations on gel phase membranes.

Keywords *Lipid bilayer – metal ions – small angle neutron diffraction – MD simulations – simulation-to-experiment analysis*

INTRODUCTION

Membranes are assemblies of mostly lipids and proteins, biomolecules which are essential to life and act as selective barriers between the cell's interior and exterior environments. In addition, these complex mesoscopic assemblies possess functions which are far more elaborate than a simple permeability barrier populated with proteins. Instead, biomembranes are highly functional dynamic machines that are central to a wide range of biological processes, including the transport of materials, cell defence, recognition, adhesion and signalling. Generally, plasma and organelle membranes serve different functions, as a result, they differ structurally (Kučerka et al., 2015a).

Cell membranes are the first line of defense against invading species, and are key to understanding disease and the efficacy of different pharmaceutical treatments. Small molecules, such as cholesterol (Marquardt et al., 2016), antimicrobial peptides (Pan et al., 2009), fusion peptides (Tristram-Nagle et al., 2010), melatonin (Drolle et al., 2013), vitamin E (Marquardt et al., 2013) and other biomolecules, are able to incorporate into the lipid matrix virtue of the membrane's structure and its associated physical properties (Marquardt et al., 2014). However, the relevant membrane structural properties associated with these processes are often controlled by the presence of certain ions, as all biological processes take place in salt solutions (Petrache et al., 2006) –i.e., the curved bilayers have been shown to undergo a series of structural changes in the presence of Ca^{2+} (Pabst et al., 2007a; Uhríková et al., 2008; Uhríková et al., 2012).

There are a number of experimental approaches used to study biomembranes at the nanoscale. Neutron scattering has proven to be a powerful technique in structural biology and biophysics (Fitter, 2006), including in studies of biological and model lipid membranes. Importantly, recent advances offer unique access to the much touted structure-function

* E-mail: kucerka@fpharm.uniba.sk

relationship in biomembranes, a relationship much sought out in biology and pharmacology (Pabst et al., 2010). Using scattering techniques, changes in the diffraction pattern can indicate important modifications to membrane structure, which may be associated with membrane function (Harroun et al., 2009). For example, small angle neutron diffraction (SAND) revealed increased levels of hydration in bacterial membranes containing Na^+ or Mg^{2+} cations, while Ca^{2+} resulted in less water penetrating the membrane (Kučerka et al., 2008b).

On the other hand, molecular dynamics (MD) simulations, are capable of providing nanoscopic details that are finer than what can be obtained by experiment. More powerful computers and better characterized force fields have made it possible to study larger and more complex systems (Ingolfsson et al., 2014). However, the data from MD simulations are a direct result of the force fields used. It is therefore essential to first validate simulation results with those obtained experimentally (Poger et al., 2016). To this end, the importance of the synergistic relationship between simulation and experiment has become very clear, where simulations are used to aid in the design of models that will ultimately be used to analyse experimental data, and in turn, experimental results are used to improve simulation force fields.

Here, we focus on the well-defined system of dipalmitoyl-phosphatidylcholine (DPPC) membranes containing calcium (Ca^{2+}) or zinc (Zn^{2+}) cations. SAND measurements of oriented multilamellar samples were analysed yielding the one-dimensional structural profile along the membrane normal. Two approaches for the analysis of neutron contrast variation measurements are discussed. In addition, the experimental results are compared to MD simulations. First, a direct simulation-to-experiment comparison was performed in scattering space (Kučerka et al., 2010), while the subsequent examination of the MD data allowed us to identify relevant regions of the membrane in real space.

MATERIALS AND METHODS

1,2-Dipalmitoyl-*sn*-glycero-3-phosphocholine (DPPC) was purchased from Avanti Polar Lipids (Alabaster, AL) and used without further purification. $CaCl_2$ and $ZnCl_2$ salts, and organic solvents were obtained from Fisher Scientific Company (Ontario). The lipid was co-solubilized with appropriate amounts of salt to achieve a stoichiometry of Me^{2+}:DPPC=1:7mol/mol. The dispersions were mixed thoroughly and deposited onto silicon wafers following a well-established procedure (Kučerka et al., 2017). The samples were held at 25 °C during the measurements in an air-tight hydration chamber, based on the original design by Katsaras (Katsaras, 1998). The chamber's bottom was filled with the saturated K_2SO_4 solution prepared at a series of D_2O/H_2O mixtures, resulting in a relative humidity (RH) of 97% (Greenspan, 1977).

Neutron diffraction data were collected at the Canadian Neutron Beam Centre's (CNBC) N5 beamline located at the National Research Universal (NRU) reactor (Chalk River, Ontario, Canada). The diffraction curves were taken using standard symmetric diffraction scans, where scattering space was probed along the *z* direction of the scattering vector *q*. The diffraction curves allow for the reconstruction of one-dimensional neutron scattering length density (NSLD) profiles, as outlined in an earlier study (Kučerka et al., 2009). In addition, rocking curves were collected to evaluate the quality of sample orientation (Nagle et al., 2016).

MD simulations using GROMACS 5.0.4 (Van Der Spoel et al., 2005) were performed at T=298 K on a system of 128 DPPC and 3655 water molecules, while the initial topology was taken from literature (Castillo et al., 2013). Me^{2+} loaded bilayers were constructed by replacing 18 of the water molecules with cations (i.e., Me^{2+}:DPPC=1:7 mol/mol). The GridMAT-MD program (Allen et al., 2009) was used to calculate an average deviation of lipid membrane thickness and an area per lipid, and the radial distribution functions were calculated using the GROMACS auxiliary program. The SIMtoEXP program (Kučerka et al., 2010) was used for the verification of simulated results with those obtained from neutron diffraction experiments.

RESULTS AND DISCUSSION

Compared to the experiment, MD simulations offer increased amounts of information at higher spatial resolution. Specifically, they allow for the identification of individual atoms within the bilayer, and map their locations in 3D space. It should be pointed out, however, that membrane systems are dynamic, and are best described by broad statistical distributions, rather than sharp delta functions typical of perfect crystals (Nagle et al., 2000). 3D simulation data were averaged in the plane of the bilayer, producing 1D distribution functions — no phase separation is expected in the 2D plane of the bilayer. Averaging was also carried out throughout the simulation production time, making the simulation results comparable to those obtained by experiment, which are also averaged over extended periods of time. Finally, we symmetrized all the distributions with respect to the bilayer centre, as any asymmetries should appear as temporary deviations. Typically, the resultant distribution functions from such an analysis are smooth curves. In addition, we combined the distribution functions of individual atoms (united atoms) into components defined by the scattering density profile (SDP) model, which described the studied DPPC bilayers (Kučerka et al., 2008a).

The probability distributions of the different components shown in Fig. 1 reveal typical features of PC bilayers. The bilayer centre is populated almost equally by methyl (CH_3) and methylene (CH_2) groups, and the CH_3 distribution is well-described by a single Gaussian. It is worth noting the absence of strong 'wings', normally seen in disordered bilayers around 15 Å from the bilayer centre (Mihailescu et al., 2011). This implies that the hydrocarbon core of our gel phase DPPC

bilayers is much more ordered. The components describing the PC head group, namely the carbonyl-glycerol (CG) and phosphate-choline (PCN), have maxima at around 17.5 Å, and 22 Å, respectively. The final component shown in Fig. 1 corresponds to the distribution of water whose amplitude achieves half maximum at ~21.6 Å. This value also indicates the lipid-water interface (i.e., the Gibbs dividing surface), or half the bilayer thickness D_B (Kučerka et al., 2008a). Together with a lipid volume of 1143.3 Å^3, as determined from our simulations using the previously derived routine (Petrache et al., 1997), we obtain a lipid area of 53 Å^2.

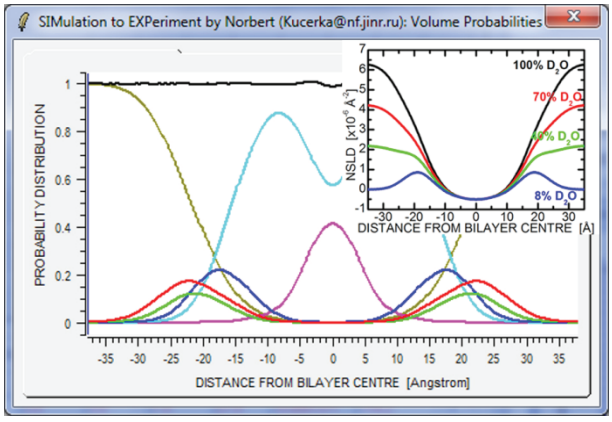

Figure 1. Volume probability distributions determined from MD simulations of neat DPPC bilayers. Atoms are grouped according to the SDP model, which consists, from the bilayer centre outwards, of methyl groups (magenta), methylene (cyan), carbonyl-glycerol (blue), PCN (i.e., phosphate+CH_2CH_2N) (red), and CholCH3 (i.e., choline's CH_3 groups) (green). The inset shows the simulation results in terms of total neutron scattering length density (NSLD) profiles calculated for various contrast conditions (i.e., 100%, 70%, 40%, and 8% D_2O).

MD simulations of systems in which Ca^{2+} or Zn^{2+} cations were added to DPPC bilayers resulted in distributions similar to those shown in Fig. 1. However, Table 1 shows that the bilayer thickness increased by about 1 Å in the case of Ca^{2+}, and decreased in the case of Zn^{2+}. A closer look at the lipid head group components reveals that these changes in bilayer thickness can be attributed to changes in the head group. Specifically, the probability distributions of both the carbonyl and phosphate groups have shifted as a result of cation addition (see Tab. 1). The location can be explained in terms of the preferential interactions between the cations, and the phosphate and carbonyl electronegative oxygens. However, the details of the interactions, which can most likely be related to differences in the electronic structures of the two ions, require further investigation.

The association of the cations with the negatively charged oxygens is further confirmed by the radial distribution functions (RDF) calculated from our simulations. Moreover, they suggest that Ca^{2+} forms contact pairs with phosphate oxygens at about twice the rate of Zn^{2+}. A similar ratio is also

Table 1. Component model structural parameters calculated from MD simulations. Total bilayer thickness D_B is calculated from the Gibbs dividing surface, while the positions of the CG and PCN components are from Gaussian fits.

	D_B [Å]	z_{CG} [Å]	z_{PCN} [Å]
DPPC neat	43.1	17.2	21.1
DPPC:Ca^{2+}	44.4	17.7	21.9
DPPC:Zn^{2+}	42.2	16.7	20.7

observed in the case of the RDF calculated for the carbonyl oxygen. In addition to confirming the preferential interactions of both cations with phosphate, these data indicate a specific binding of Ca^{2+} with the phosphate group, while suggesting a much weaker binding between Zn^{2+} and all other atoms within the lipid head group (Kučerka et al., 2017).

Although our MD results have provided us with some very interesting physical insights, the overall bilayer structural parameters are better determined by experiment. The shortcomings of the different force fields have been previously discussed, particularly with respect to the determination of area per lipid (Kučerka et al., 2010; Valley et al., 2011; Poger et al., 2016). We conducted SAND measurements on the same system as was used for MD simulations to validate the above discussed results. SAND experiments involved contrast variation measurements in which a series of contrast solutions (i.e., 100%, 70%, 40% and 8% D_2O/H_2O) were used. This approach allowed us to solve the scattering phase problem by requiring the scattering form factors to change linearly as a function of D_2O content. The rule arises from the fact that for centro-symmetric systems (as those studied here) scattering intensity is proportional to the square of the contrast between the measured object and the solvent, (Worcester et al., 1976). Once the form factors and their signs are determined, the neutron scattering length density (NSLD) profile is calculated by Fourier transformation (Kučerka et al., 2009). Except for the assumption that the bilayers are centrosymmetric, this procedure inverts the data from reciprocal space into real space without any further assumptions. The 100% D_2O contrast condition provides the best estimate of bilayer steric thickness, while lower contrast profiles reveal more details of the lipid head group region (see inset to Fig. 1). In addition, the contrast varied diffraction data can be subtracted from each other, providing water probability distributions similar to those obtained from MD simulations (Kučerka et al., 2009). Fig. 2 compares these distributions for all three bilayers studied.

Comparison of the simulated and experimental results indicates small differences. Although the simulated data suggest a thickening of the bilayer in the presence of Ca^{2+} ion binding, and a slight decrease in the case of Zn^{2+}, experimental data show a similar effect for both ions. This observation is consistent with previously published results, whereby

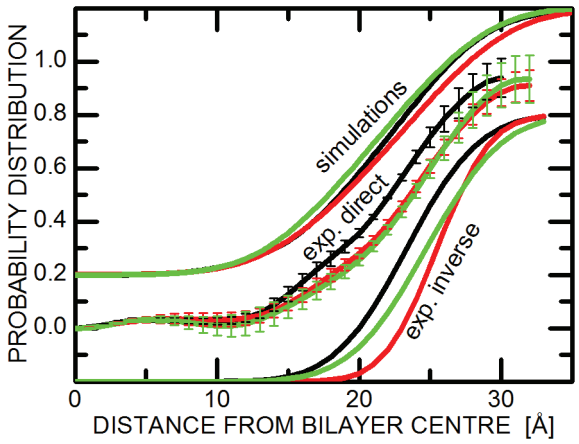

Figure 2. Water probability distributions from simulations (curves shifted up) and by analysis of the experimental data, in real (exp. direct) and reciprocal space (exp. inverse; curves shifted down). The different coloured curves show results for neat DPPC bilayers (black) and those containing Ca^{2+} (red) or Zn^{2+} (green) cations.

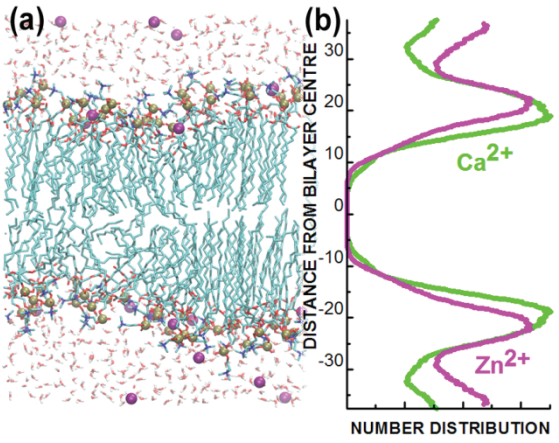

Figure 3. (a) Simulation snapshot of DPPC+Zn^{2+} bilayers showing some of the hydrocarbon chains (low-left part) in the disordered fluid phase, despite a simulation temperature T=298K. (b) The number distribution of Ca^{2+} and Zn^{2+} cations across the DPPC bilayers.

zwitterionic lipid multilayers tend to swell in the presence of salts (Yamada et al., 2005; Petrache et al., 2006; Pabst et al., 2007b; Alsop et al., 2016).

As mentioned, analysis of experimental data in real space does not require any assumptions regarding the NSLD profile functional form, nor of the probability distributions resulting from direct subtraction. The water distribution is obtained from averaging the different contrast varied NSLD profile subtracted pairs, which also provide an estimate of the standard deviation error (Fig. 2). It should be pointed out that these results are, for the most part, qualitative. We used a different approach to analyse the experimental data, producing more quantitative results. This approach evaluates all the different contrast diffraction data simultaneously, while assuming that water probability follows the error function (Kučerka et al., 2009). Results in Fig. 2 show good agreement between the two methods of data analysis. However, our data also highlights the differences between experiment and simulation.

The accuracy of MD simulations is known to vary from study to study, depending on the force field used and the treatment of the electrostatics (Pan et al., 2012). The most difficult aspect for simulations is in reproducing the global membrane parameters due to an imbalance of long range interactions and their approximations, and truncations in the calculations (Kučerka et al., 2015b). As a result, many simulations require an extra variable parameter (e.g., temperature, partial charges, area or surface tension) in order to converge with experiment. For example, we noticed an increased level of disorder in some of the hydrocarbon chains (Fig. 3a), suggesting the spontaneous formation of short-lived fluid phase bilayer regions. This was especially true at the beginning of the simulations. Even though the ordered phase was established during the production run, some fluctuations or other secondary effects may have worked themselves in to our final results.

It is recognized and accepted that atomic-level simulations can provide quantitative details that surpass those obtained from the experiment. These molecular details offer insights into the nature of short-range interactions, hydrogen bridges, and binding specificity. Interatomic correlations also fall into this category, from which we calculated the RDFs between cations and several different atoms within the lipid head group. The data in Fig. 3b shows the presence of strong correlations between Ca^{2+} and the phosphate electronegative oxygen, and also points to the fact that Zn^{2+} cations bind weaker than Ca^{2+} cations (Kučerka et al., 2017). In addition to the RDF results that shed light on the differences between the two cations, the distribution functions agree well with the experimentally obtained results. Despite their subtle differences, Ca^{2+} and Zn^{2+} seem to affect the structural properties of gel phase DPPC bilayers similarly at the concentration examined.

CONCLUSIONS

We used MD simulations and SAND to determine the structural details of DPPC: bilayers containing Ca^{2+} and Zn^{2+} at a lipid:metal molar ratio of 7:1. Simulations were compared to experiments using the simulation-to-experiment approach. Although there is good agreement between simulation and experimental results, SIMtoEXP also shows discrepancies between the two. These differences are not unexpected, and are most likely the result of a less than perfect MD force field. As a result, experimental data were used to determine the overall bilayer structures, which suggest that the addition

of either Ca^{2+} or Zn^{2+} cations induces bilayers to swell. MD simulations, on the other hand, decomposed the bilayer into smaller structural subunits, allowing us to extract important information regarding short-range interactions. It seems that both cations are attracted to the electronegative phosphate and carbonyl moieties of the PC head group. However, Ca^{2+} seems to display an enhanced binding affinity for the phosphate group. Finally, the effects on the bilayer's structural properties at the DPPC:Me^{2+} ratio studied are the same for both cations.

ACKNOWLEDGEMENT

The authors acknowledge support from VEGA grant 1/0916/16, APVV-0212-10, JINR project 04-4-1121-2015/2017, and access to CINS experimental facility and JINR computational heterogeneous cluster HybriLIT. J. K. acknowledges the support received through the Department of Energy (DOE) Scientific User Facilities Division, Office of Basic Energy Sciences (contract no. DEAC05-00OR2275), and funding from the Laboratory Directed Research and Development program.

References

[1] Allen, W. J., Lemkul, J. A., and Bevan, D. R. GridMAT-MD: a Grid-Based Membrane Analysis Tool for Use With Molecular Dynamics. J.Comput.Chem. 2009;30(12):1952-8.

[2] Alsop, R. J., Maria, Schober R., and Rheinstadter, M. C. Swelling of Phospholipid Membranes by Divalent Metal Ions Depends on the Location of the Ions in the Bilayers. Soft Matter 10-8-2016;12(32):6737-48.

[3] Castillo, N., Monticelli, L., Barnoud, J., and Tieleman, D. P. Free Energy of WALP23 Dimer Association in DMPC, DPPC, and DOPC Bilayers. Chem.Phys Lipids 2013;169:95-105.

[4] Drolle, E., Kučerka, N., Hoopes, M. I., Choi, Y., Katsaras, J., Karttunen, M., and Leonenko, Z. Effect of Melatonin and Cholesterol on the Structure of DOPC and DPPC Membranes. Biochimica et Biophysica Acta 2013;1828(9):2247-54.

[5] Fitter, J., Neutron scattering in biology: Techniques and applicationsSpringer-Verlag; 2006.(Gutberlet, T.; Katsaras, J.

[6] Greenspan, Lewis. Humidity Fixed Points of Binary Saturated Aqueous Solutions. JOURNAL OF RESEARCH of the National Bureau of Standards - A.Phys ics and Chemistry 1977;81A(1):89-96.

[7] Harroun, Thad A., Kučerka, Norbert, Nieh, Mu Ping, and Katsaras, John. Neutron and X-Ray Scattering for Biophysics and Biotechnology: Examples of Self-Assembled Lipid Systems. Soft Matter 2009;5(14):2694-703.

[8] Ingolfsson, H. I., Melo, M. N., van Eerden, F. J., Arnarez, C., Lopez, C. A., Wassenaar, T. A., Periole, X., de Vries, A. H., Tieleman, D. P., and Marrink, S. J. Lipid Organization of the Plasma Membrane. J.Am.Chem.Soc. 15-10-2014;136(41):14554-9.

[9] Katsaras, J. Adsorbed to a Rigid Substrate, Dimyristoylphosphatidylcholine Multibilayers Attain Full Hydration in All Mesophases. Biophys.J. 1998;75(5):2157-62.

[10] Kučerka, N., Heberle, F. A., Pan, J., and Katsaras, J. Structural Significance of Lipid Diversity As Studied by Small Angle Neutron and X-Ray Scattering. Membranes (Basel) 2015a;5(3):454-72.

[11] Kučerka, N., Katsaras, J., and Nagle, J. F. Comparing Membrane Simulations to Scattering Experiments: Introducing the SIMtoEXP Software. Journal of Membrane Biology 2010;235(1):43-50.

[12] Kučerka, N., Nagle, J. F., Sachs, J. N., Feller, S. E., Pencer, J., Jackson, A., and Katsaras, J. Lipid Bilayer Structure Determined by the Simultaneous Analysis of Neutron and X-Ray Scattering Data. Biophys.J. 2008a;95(5):2356-67.

[13] Kučerka, N., Nieh, M. P., Pencer, J., Sachs, J. N., and Katsaras, J. What Determines the Thickness of a Biological Membrane. Gen. Physiol Biophys. 2009;28(2):117-25.

[14] Kučerka, N., Papp-Szabo, E., Nieh, M. P., Harroun, T. A., Schooling, S. R., Pencer, J., Nicholson, E. A., Beveridge, T. J., and Katsaras, J. Effect of Cations on the Structure of Bilayers Formed by Lipopolysaccharides Isolated From Pseudomonas Aeruginosa PAO1. J.Phys Chem.B 10-7-2008b;112(27):8057-62.

[15] Kučerka, N., van Oosten, B., Pan, J., Heberle, F. A., Harroun, T. A., and Katsaras, J. Molecular Structures of Fluid Phosphatidylethanolamine Bilayers Obtained From Simulation-to-Experiment Comparisons and Experimental Scattering Density Profiles. The Journal of Physical Chemistry B 5-2-2015b;119(5):1947-56.

[16] Kučerka, N., Dushanov, E., Kholmurodov, K. T., Katsaras, J., and Uhríková, D. Calcium and Zinc Differentially Affect the Structure of Lipid Membranes. Langmuir 2017;33:3134-3141.

[17] Marquardt, D., Kučerka, N., Wassall, S. R., Harroun, T. A., and Katsaras, J. Cholesterol's Location in Lipid Bilayers. Chem.Phys Lipids 2016;199:17-25.

[18] Marquardt, D., Williams, J. A., Kučerka, N., Atkinson, J., Wassall, S. R., Katsaras, J., and Harroun, T. A. Tocopherol Activity Correlates With Its Location in a Membrane: a New Perspective on the Antioxidant Vitamin E. J.Am.Chem.Soc. 22-5-2013;135(20):7523-33.

[19] Marquardt, Drew; Harroun, Thad A. Locations of Small Biomolecules in Model Membranes. Liposomes, Lipid Bilayers and Model Membranes.CRC Press; 19-2-2014. pp.199-216.

[20] Mihailescu, M., Vaswani, R. G., Jardon-Valadez, E., Castro-Roman, F., Freites, J. A., Worcester, D. L., Chamberlin, A. R., Tobias, D. J., and White, S. H. Acyl-Chain Methyl Distributions of Liquid-Ordered and -Disordered Membranes. Biophys.J. 16-3-2011;100(6):1455-62.

[21] Nagle, J. F., Akabori, K., Treece, B. W., and Tristram-Nagle, S. Determination of Mosaicity in Oriented Stacks of Lipid Bilayers. Soft Matter 14-2-2016;12(6):1884-91.

[22] Nagle, J. F. and Tristram-Nagle, S. Structure of Lipid Bilayers. Biochimica et Biophysica Acta 10-11-2000;1469(3):159-95.

[23] Pabst, G., Hodzic, A., Strancar, J., Danner, S., Rappolt, M., and Laggner, P. Rigidification of Neutral Lipid Bilayers in the Presence of Salts. Biophys.J. 15-10-2007a;93(8):2688-96.

[24] Pabst, G., Hodzic, A., Strancar, J., Danner, S., Rappolt, M., and Laggner, P. Rigidification of Neutral Lipid Bilayers in the Presence of Salts. Biophys.J. 15-10-2007b;93(8):2688-96.

[25] Pabst, G., Kučerka, N., Nieh, M. P., Rheinstadter, M. C., and Katsaras, J. Applications of Neutron and X-Ray Scattering to the Study of Biologically Relevant Model Membranes. Chem.Phys Lipids 2010;163(6):460-79.

[26] Pan, J., Heberle, F. A., Tristram-Nagle, S., Szymanski, M., Koepfinger, M., Katsaras, John, and Kučerka, N. Molecular Structures of Fluid Phase Phosphatidylglycerol Bilayers As Determined by Small Angle Neutron and X-Ray Scattering. Biochimica et Biophysica Acta 2012;1818(9):2135-48.

[27] Pan, J., Tristram-Nagle, S., and Nagle, J. F. Alamethicin Aggregation in Lipid Membranes. Journal of Membrane Biology 2009;231(1):11-27.

[28] Petrache, H. I., Feller, S. E., and Nagle, J. F. Determination of Component Volumes of Lipid Bilayers From Simulations. Biophys.J. 1997;72(5):2237-42.

[29] Petrache, H. I., Tristram-Nagle, S., Harries, D., Kučerka, N., Nagle, J. F., and Parsegian, V. A. Swelling of Phospholipids by Monovalent Salt. J.Lipid Res. 2006;47(2):302-9.

[30] Poger, D., Caron, B., and Mark, A. E. Validating Lipid Force Fields Against Experimental Data: Progress, Challenges and Perspectives. Biochimica et Biophysica Acta 2016;1858(7 Pt B):1556-65.

[31] Tristram-Nagle, S., Chan, R., Kooijman, E., Uppamoochikkal, P., Qiang, W., Weliky, D. P., and Nagle, J. F. HIV Fusion Peptide Penetrates, Disorders, and Softens T-Cell Membrane Mimics. J.Mol.Biol. 10-9-2010;402(1):139-53.

[32] Uhríková, D., Kučerka, N., Lengyel, A., Pullmannová, P., Teixeira, J., Murugova, T., Funari, S. S., and Balgavý, P. Lipid Bilayer - DNA Interaction Mediated by Divalent Metal Cations: SANS and SAXD Study. Journal of Physics: Conference Series 2012;351(1):012011.

[33] Uhríková, D., Kučerka, N., Teixeira, J., Gordeliy, V., and Balgavý, P. Structural Changes in Dipalmitoylphosphatidylcholine Bilayer Promoted by Ca2+ Ions: a Small-Angle Neutron Scattering Study. Chem.Phys Lipids 2008;155(2):80-9.

[34] Valley, C. C., Perlmutter, J. D., Braun, A. R., and Sachs, J. N. NaCl Interactions With Phosphatidylcholine Bilayers Do Not Alter Membrane Structure but Induce Long-Range Ordering of Ions and Water. Journal of Membrane Biology 2011;244(1):35-42.

[35] Van Der Spoel, D., Lindahl, E., Hess, B., Groenhof, G., Mark, A. E., and Berendsen, H. J. GROMACS: Fast, Flexible, and Free. J.Comput.Chem. 2005;26(16):1701-18.

[36] Worcester, D. L. and Franks, N. P. Structural Analysis of Hydrated Egg Lecithin and Cholesterol Bilayers. II. Neutrol Diffraction. J.Mol.Biol. 25-1-1976;100(3):359-78.

[37] Yamada, L., Seto, Hideki, Takeda, Takayoshi, Nagao, Michihiro, Kawabata, Youhei, and Inoue, Katsuaki. SAXS, SANS and NSE Studies on "Unbound State" in DPPC/Water/CaCl2 System. Journal of the Physical Society of Japan 15-10-2005;74(10):2853-9.

DE GRUYTER OPEN

Eur. Pharm. J. 2017, 64 (2): 15-21.
ISSN 1338-6786 (online) and ISSN 2453-6725 (print version),
DOI: 10.1515/afpuc-2017-0019

EUROPEAN PHARMACEUTICAL JOURNAL

Regulation of the $Ca_V3.2$ calcium channels in health and disease
Regulácia $Ca_V3.2$ vápnikových kanálov v zdraví a chorobe

Original Paper

Lacinová Ľ.[1,2]✉

[1]Slovak Academy of Sciences, Centre of Bioscience, Bratislava, Slovak Republic
[2]University of Ss. Cyril and Methodius in Trnava, Faculty of Natural Sciences, Trnava, Slovak Republic

/

[1]Slovenská akadémia vied, Biomedicínske centrum SAV, Bratislava, Slovenská Republika
[2]Univerzita sv. Cyrila a Metoda v Trnave, Fakulta prírodných vied, Trnava, Slovenská Republika

Received 24 October, 2016, accepted 16 March, 2017

Abstract Family of T-type or low-voltage activated calcium channels consists of three members: $Ca_V3.1$, $Ca_V3.2$, and $Ca_V3.3$. $Ca_V3.2$ channel has almost identical biophysical properties as the $Ca_V3.1$ channel, but is distinguished by a specific tissue expression profile and a prominent role in several pathologies, including neuropathic pain, epilepsy, and dysregulation of cardiac rhythm. Further, it may be involved in phenotype of autism spectrum disorders, and amyotrophic lateral sclerosis. It represents a promising target for future pharmacotherapies.

Slovak abstract Skupina nízkonapäťových vápnikových kanálov nazývaných aj kanály T-typu má troch členov: $Ca_V3.1$, $Ca_V3.2$, a $Ca_V3.3$. $Ca_V3.2$ kanál má temer identické biofyzikálne vlastnosti ako $Ca_V3.1$ kanál, ale líši sa od neho tým, že je exprimovaný v iných tkanivách a má dôležitú úlohu pri viacerých závažných ochoreniach ako sú neuropatická bolesť, epilepsia a poruchy regulácie srdcového rytmu. Preto tento kanál môže byť cieľom nových liečiv.

Keywords *T-type calcium channel – $Ca_V3.2$ – regulation – trafficking – glycosylation*

Kľúčové slová: *vápnikové kanály T-typu – regulácia $Ca_V3.2$ kanála – transport do membrány – glykozylácia*

INTRODUCTION

T-type calcium channels, also known as low-voltage-activated calcium channels, or Ca_V3 channels, are characterised by a relatively negative voltage activation threshold around -60 mV. This feature enables them to operate near the resting membrane potential of most electrically excitable cells and contribute to the initiation of an action potential. T-type calcium channels play a fundamental role in shaping neuronal excitability, as they generate the so-called low threshold calcium action potential in neurons lacking sodium channels and support burst firing (Perez-Reyes, 2003). In the heart, they contribute to the pacemaker function of sinoatrial nodal cells. Three subtypes of Ca_V3 channels are currently known: $Ca_V3.1$, $Ca_V3.2$ and $Ca_V3.3$, with α_1 subunits encoded by CACNA1G, CACNA1H, and CACNA1I genes (Lacinova et al., 2000) 2000. $Ca_V3.1$ and $Ca_V3.2$ channels share the basic biophysical properties, for example, kinetics of activation and inactivation (Figure 1 A), voltage dependence of activation and inactivation (Figure 1 B), and kinetics of recovery from an inactivation (Lacinova, 2005). $Ca_V3.3$ channels have distinguished biophysical properties (Chemin et al., 2002) having one decimal order slower activation and inactivation kinetics (Figure 1 A), but virtually identical voltage dependence of activation (Figure 1 B) compared to the $Ca_V3.1$ and $Ca_V3.2$ channels. These channels are expressed almost exclusively in the brain (Monteil et al., 2000). $Ca_V3.1$ and $Ca_V3.2$ channels are ubiquitously expressed; nevertheless, their expression patterns only partly overlap in the mammalian brain (Lacinova, 2004; Aguado et al., 2016) and throughout the mammalian body at large. In addition to neuronal tissue, $Ca_V3.2$ was identified in the heart (Cribbs et al., 1998), skeletal muscle (Berthier et al., 2002), pancreas (Braun et al., 2008), kidney (Hayashi et al., 2007), and also in female (Ohkubo et al., 2005), and male reproductive tissues (Darszon et al., 2006).

* *E-mail: lubica.lacinova@savba.sk*

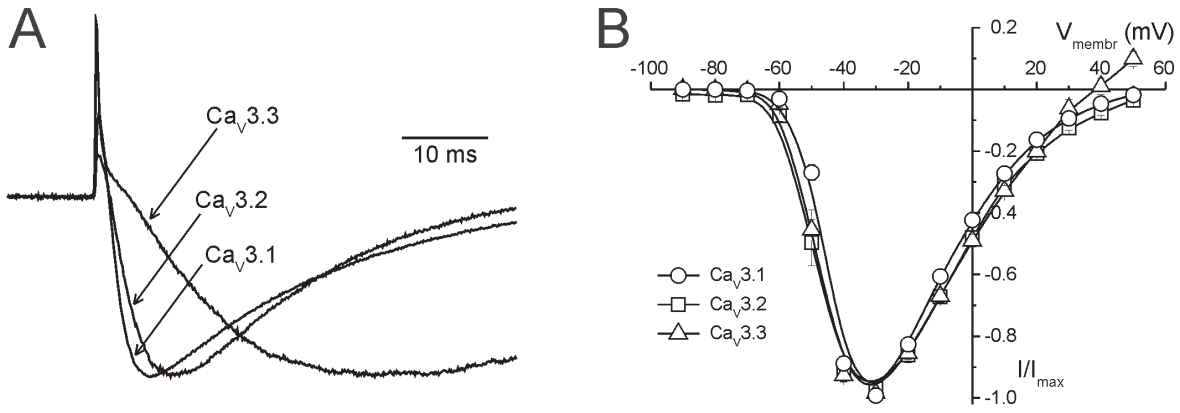

Figure 1. Basic biophysical profile of T-type calcium channels. a. Examples of current traces activated by a rectangular depolarising pulse from a potential of -100 mV to a -20 mV. Traces corresponding to individual channel subtypes ($Ca_V3.1$, $Ca_V3.2$, and $Ca_V3.3$) are marked. b. Current-voltage relations for all three subtypes ($Ca_V3.1$, $Ca_V3.2$, and $Ca_V3.3$) of T-type calcium channel, as marked.

The altered function of T-type calcium channels was implied in several pathological states. $Ca_V3.2$ channels seem to be of a particular importance as they were implied in several heritable diseases.

$CA_V3.2$ CHANNELS IN NEURONS

Typical resting membrane potential of most neurons corresponds to a voltage range at which T-type calcium channels are partly inactivated. Minor hyperpolarisation recruits additional T-type calcium channels, enhances T-type calcium current and enables the generation of low-threshold action potentials. Low-threshold action potentials form the backbone for neuronal burst firing (Huguenard, 1998). Ability of Ca_V3 channels to initiate an action potential firing may contribute to epileptiform activity. Indeed, mutations in $Ca_V3.2$ channel were associated with the childhood absence epilepsy (Chen et al., 2003) and with other forms of idiopathic generalised epilepsy (Heron et al., 2004; Heron et al., 2007). Identified mutations were either gain-of-function or did not alter electrophysiological properties of the channel. Mechanism by which these mutations increase neuronal excitability, and subsequently increase seizure susceptibility, was investigated (Eckle et al., 2014). These authors suggested that increased current density caused by an epilepsy mutation C456S may be at least partly due to the increased surface expression of $Ca_V3.2$ channels. Further, this mutation enhanced glutamatergic transmission by the enhancement of local calcium influx at synapses (Wang et al., 2015). It is interesting that in spite of that, $Ca_V3.1$ channel has the same electrophysiological profile as $Ca_V3.2$ channel, $Ca_V3.1^{-/-}$ mice are resistant to baclofen-induced epilepsy (Kim et al., 2001), and overexpression of $Ca_V3.1$ channel induced absence epilepsy in mice (Ernst et al., 2009), no consistent linkage of this channel to epilepsy was found until now.

Autism spectrum disorders (ASD) represent complex neurodevelopmental conditions. Causes of ASD remain a mystery, however, heritable components were demonstrated (Zoghbi, 2003). Interestingly, mutations in voltage-dependent calcium channels associated with ASD were reported. Initially, the gain-of-function mutation of $Ca_V1.2$ L-type calcium channel was described by Splawski and coauthors (Splawski et al., 2004; Splawski et al., 2005). Soon, a group led by the same authors reported four loss-of-function point mutations in $Ca_V3.2$ channel, associated with ASD (Splawski et al., 2006). How an altered conductance of $Ca_V3.2$ channels arising from these mutations may lead to ASD phenotype remains unknown.

Two rare recessive variants of the CACNA1H gene associated with sporadic amyotrophic lateral sclerosis (ALS) were recently discovered (Steinberg et al., 2015). When these missense mutations (V1689M and A1705T) were introduced into recombinant channels and expressed, they produced moderate but significant changes in the channel properties consistent with loss-of-function of the mutated channel (Rzhepetskyy et al., 2016). Mathematical modelling suggested that these changes may result in decreased excitability of thalamic neurons (Rzhepetskyy et al., 2016).

Key role of neuronally expressed $Ca_V3.2$ channels in nociception was established (Todorovic and Jevtovic-Todorovic, 2013). Downregulation of these channels in rat dorsal root ganglion neurons resulted in major antinociceptive, anti-hyperalgesic, and anti-allodynic effects (Bourinet et al., 2005). Inhibition of $Ca_V3.2$ channels contributed to antinociceptive effect of epipregnanolone (Ayoola et al., 2014), KYS-05090S (M'Dahoma et al., 2016), and to the peripheral anti-nociceptive effect of substance P (Huang et al., 2016). $Ca_V3.2$ channel emerged as a prospective target of future analgesics.

$CA_V3.2$ CHANNELS IN THE CARDIOVASCULAR SYSTEM

$Ca_V3.2$ channel gene CACNA1H was originally cloned from a human heart by a screening of cDNA library with the $Ca_V3.1$ gene (Cribbs et al., 1998). These channels are expressed in

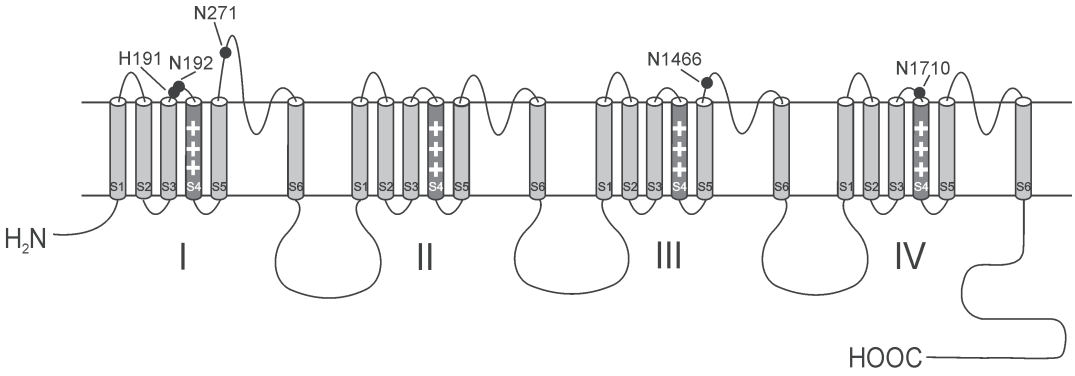

Figure 2. Scheme of T-type α1 subunit. α1 subunit of T-type calcium channel consists of four homological domains (I – IV). Each domain consists of six transmembrane segments S1–S6. S4 segment contains 5–6 positively charged amino acids and is responsible for voltage sensing. Segments S5–S6 create conducting pore of the channel. Location of histidine 191 (H191) and four extracellularly located asparagines (N192, N271, N1466, and N1710) are marked by filled circles.

ventricular myocytes, where they mediate chronotropic action of corticosteroids (Maturana et al., 2009) and aldosterone (Lalevee et al., 2005). In sinoatrial nodal cells, $Ca_V3.2$ channels contribute to cardiac pacemaking due to their ability to be activated during initial slow depolarising phase of sinoatrial action potential, which enables them to contribute to this depolarisation process (Husse and Franz, 2016). Their expression in sinoatrial cells is increased in streptozotocin-induced diabetic rats (Ferdous et al., 2016) and thus, they may contribute to cardiac-related comorbidity in diabetic patients. Recently, gain-of-function mutation CACNA1H(M1549V) of the $Ca_V3.2$ channel was identified, which results in an early onset hypertension caused by increased aldosterone production (Scholl et al., 2015).

REGULATION OF $CA_V3.2$ CHANNELS BY GASOTRANSMITTERS

Gasotransmitters, such as nitric oxide, carbon monoxide and hydrogen sulphide may act as calcium channel modulators. In recent years, (patho)physiological importance of H_2S is being acknowledged (Li et al., 2011). Acutely applied micromolar H_2S inhibited the current through the recombinant $Ca_V3.2$ channel, but not through $Ca_V3.1$ or $Ca_V3.3$ channels (Elies et al., 2014). It was shown that H_2S interacts with the $Ca_V3.2$ channel at an amino acid histidine in a position 191 (H191, Figure 2), which is absent in $Ca_V3.1$ and $Ca_V3.3$ channels (Elies et al., 2015). The same amino acid residue is responsible for channel inhibition by Zn^{2+} (Nelson et al., 2007), by Ni^{2+} (Kang et al., 2006), and for redox regulation of the channel. Elies and coauthors suggested that H_2S may enhance channel sensitivity to Zn^{2+} ions (Elies et al., 2016). However, chronic exposure to millimolar H_2S enhanced T-type calcium current in NG108-15 cells and evoked hyperalgesia in rats (Kawabata et al., 2007). Acute augmentation of the current through recombinant $Ca_V3.2$, but not $Ca_V3.1$ channel was also achieved by millimolar H_2S (Elies et al., 2014). Mechanism of this dual effect remains unknown.

Carbon monoxide inhibited all three recombinant Ca_V3 channels and reached half-maximal inhibition in concentration around 3 μM (Boycott et al., 2013). The effect of nitric monoxide on T-type calcium channels was not investigated.

REGULATION OF $CA_V3.2$ CHANNELS BY OTHER ENDOGENOUS MOLECULES

T-type channels are also sensitive to a number of endogenous agents. For instance, arachidonic acid potently shifts the steady-state inactivation of $Ca_V3.2$ channels by -25 mV, eliminating the window current (Zhang et al., 2000). Considering that arachidonic acid is used in a number of anabolic bodybuilding supplements, the alteration of immune response may represent a side effect of these products. Endogenous cannabinoid anandamide inhibits all three Ca_V3 channels with order of efficiency $Ca_V3.2 > Ca_V3.3 > Ca_V3.1$ (Chemin et al., 2001). Inhibition of $Ca_V3.2$ channels by endocannabinoid N-arachidonoyl dopamine (Ross et al., 2009), by endogenous lipoamino acids (Barbara et al., 2009), and by N-arachidonoyl serotonin (Gilmore et al., 2012) may contribute to their anti-nociceptive effect attributed to the interaction with TRPV1 channel.

REGULATION OF $CA_V3.2$ CHANNELS BY GLUCOSE

Glycosylation represents one of the most prevalent mechanisms of post-translational modification of proteins (Moremen et al., 2012). It is reversible and proteins can undergo dynamic glycosylation and deglycosylation. Asparagine (N)-linked glycosylation of various voltage- and ligand-gated channels (Ufret-Vincenty et al., 2001; Watanabe et al., 2003; Cohen, 2006) including $Ca_V3.2$ channel (Weiss et al., 2013) was documented. Consensus N-linked glycosylation site has an amino acid sequence N-*X*-S/T. Four corresponding asparagines are located in the extracellular loops of the $Ca_V3.2$ channel: N192, N271, N1466 and N1710 (Figure 2). Inhibition of N-linked glycosylation by tunicamycin reduced an expression

of the $Ca_V3.2$ channel in cell membrane (Weiss et al., 2013) and reduced the current density. Increase of extracellular glucose concentration from 5 mM (physiological level) to 25 mM (corresponding to clinically observed hyperglycaemia) potentiated the trafficking of channel protein to the plasma membrane (Lazniewska et al., 2016) and increased the current density (Weiss et al., 2013). An uneven role of glycosylation of individual asparagines was demonstrated by a substitution of each asparagine by glutamine. Mutations N271Q and N1710Q disrupted the channel expression and no detectable current was observed in cells transfected with these constructs (Weiss et al., 2013; Ondacova et al., 2016). Total protein expression of N192Q and N1466Q channels was unaffected but their trafficking to the surface membrane was decreased (Weiss et al., 2013). Glycosylation could regulate the current amplitude solely by altering the number of functional channel expressed in the plasma membrane. Alternatively, changes in channel gating could contribute to decreased current amplitude. To test for involved mechanisms, the charge movement in wild type and mutant channels was investigated by Ondacova and coauthors. The charge movement arises from upwards movement of S4 segments in all four channel domains (Figure 2) and is proportional to the number of functional channels in a cell membrane. Ratio maximal current/maximal charge movement is proportional to the channel opening probability (Agler et al., 2005). Individual mutations (N192Q or N1466Q) did not alter this ratio significantly. However, when both asparagines were replaced by glutamines, the ratio maximal current/maximal charge movement decreased significantly, suggesting that proper glycosylation of the $Ca_V3.2$ channel may also upregulate the channel's opening probability (Ondacova et al., 2016). Considering that the elevated glucose caused the enhanced activity of $Ca_V3.2$ channels, which plays an important role in the peripheral nociception, this mechanism may be involved in the genesis of diabetic neuropathy. Therefore, these channels are emerging targets for its therapy (Orestes et al., 2013).

REGULATION OF THE $CA_V3.2$ CHANNELS BY PHOSPHORYLATION

$Ca_V3.2$ channels are regulated by multiple phosphorylation mechanisms. Using high resolution mass spectroscopy, 34 putative phosphorylation sites, represented by serine and threonine residues, were identified in the intracellular loops of the rat $Ca_V3.2$ channel and 43 such sites were identified in the human $Ca_V3.2$ channel (Blesneac et al., 2015). Dephosphorylation of the channel by non-specific phosphatase AP accelerated its activation and inactivation kinetics, and shifted the voltage dependencies of channel activation and inactivation in hyperpolarising direction (Blesneac et al., 2015). Several of these phosphorylation sites were described previously. S1198 in the cytoplasmic loop, connecting the channel domains II and III, is phosphorylated by CaMKII (Welsby et al., 2003; Yao et al., 2006). This amino acid residue is unique to the CACNA1H sequence (Perez-Reyes, 2003). Its phosphorylation potentiates calcium entry through the $Ca_V3.2$ channels by shifting the half-maximal activation voltage towards the more negative membrane potentials and by increasing voltage sensitivity of the channel (Welsby et al., 2003). Phosphorylation of S1107 located in the same intracellular loop by protein kinase A is necessary for channel inhibition by Gβγ dimers (Hu et al., 2009). This signalling pathway is specific for the $Ca_V3.2$ channel and may be a mechanism mediating dopamine inhibition of this channel (Hu et al., 2009).

Vast majority of experiments are conducted at a room temperature. Chemin and coauthors demonstrated that protein kinases A and C, but not G, can enhance the current through all three Ca_V3 channel subtypes at a physiological temperature (30–37 °C), while no effect was observed at room temperature (20–27 °C) (Chemin et al., 2007). This observation should be taken into account when we think about regulation of T-type calcium current in a mammalian organism.

REGULATION OF THE $CA_V3.2$ CHANNELS BY UBIQUITINATION

Ubiquitination is a common enzymatic post-translational modification of proteins occurring in eukaryotic cells. $Ca_V3.2$ channels are under control by ubiquitinating and deubiquitinating enzymes as well (Zamponi et al., 2015). Deubiquitination of the $Ca_V3.2$ channel by deubiquitinase USP5 results in an increased T-type calcium current that is responsible for inflammatory and neuropathic pain (Gadotti et al., 2015). Disrupting USP5/$Ca_V3.2$ channel interactions prevented such pain and represents a concept for a new class of analgesics (Garcia-Caballero et al., 2014; Gadotti et al., 2015; Garcia-Caballero et al., 2016).

CONCLUSION

$Ca_V3.2$ channels play a unique role in nociception, in heart automaticity, in several types of epilepsy and convulsion. They may be involved in diabetic neuropathy, autism spectrum disorders, or amyotrophic lateral sclerosis. These features make them valuable pharmacological targets.

ACKNOWLEDGEMENT

While working on this manuscript, LL was supported by VEGA 2/0107/16 grant.

References

[1] Agler HL, Evans J, Tay LH, Anderson MJ, Colecraft HM, Yue DT. G protein-gated inhibitory module of N-type ($Ca_v2.2$) Ca^{2+} channels. Neuron. 2005; 46:891-904.

[2] Aguado C, Garcia-Madrona S, Gil-Minguez M, Lujan R. Ontogenic Changes and Differential Localization of T-type Ca(2+) Channel Subunits Cav3.1 and Cav3.2 in Mouse Hippocampus and Cerebellum. Front Neuroanat. 2016; 10:83.

[3] Ayoola C, Hwang SM, Hong SJ, Rose KE, Boyd C, Bozic N, Park JY, Osuru HP, DiGruccio MR, Covey DF, Jevtovic-Todorovic V, Todorovic SM. Inhibition of CaV3.2 T-type calcium channels in peripheral sensory neurons contributes to analgesic properties of epipregnanolone. Psychopharmacology (Berl). 2014; 231:3503-15.

[4] Barbara G, Alloui A, Nargeot J, Lory P, Eschalier A, Bourinet E, Chemin J. T-type calcium channel inhibition underlies the analgesic effects of the endogenous lipoamino acids. J Neurosci. 2009; 29:13106-14.

[5] Berthier C, Monteil A, Lory P, Strube C. Alpha(1H) mRNA in single skeletal muscle fibres accounts for T-type calcium current transient expression during fetal development in mice. J Physiol. 2002; 539:681-91.

[6] Blesneac I, Chemin J, Bidaud I, Huc-Brandt S, Vandermoere F, Lory P. Phosphorylation of the Cav3.2 T-type calcium channel directly regulates its gating properties. Proc Natl Acad Sci U S A. 2015; 112:13705-10.

[7] Bourinet E, Alloui A, Monteil A, Barrere C, Couette B, Poirot O, Pages A, McRory J, Snutch TP, Eschalier A, Nargeot J. Silencing of the Cav3.2 T-type calcium channel gene in sensory neurons demonstrates its major role in nociception. EMBO J. 2005; 24:315-24.

[8] Boycott HE, Dallas ML, Elies J, Pettinger L, Boyle JP, Scragg JL, Gamper N, Peers C. Carbon monoxide inhibition of Cav3.2 T-type Ca2+ channels reveals tonic modulation by thioredoxin. FASEB J. 2013; 27:3395-407.

[9] Braun M, Ramracheya R, Bengtsson M, Zhang Q, Karanauskaite J, Partridge C, Johnson PR, Rorsman P. Voltage-gated ion channels in human pancreatic beta-cells: electrophysiological characterization and role in insulin secretion. Diabetes. 2008; 57:1618-28.

[10] Cohen DM. Regulation of TRP channels by N-linked glycosylation. Semin Cell Dev Biol. 2006; 17:630-7.

[11] Cribbs LL, Lee JH, Yang J, Satin J, Zhang Y, Daud A, Barclay J, Williamson MP, Fox M, Rees M, Perez-Reyes E. Cloning and characterization of a_{1H} from human heart, a member of the T-type Ca^{2+} channel gene family. Circ Res. 1998; 83:103-9.

[12] Darszon A, Lopez-Martinez P, Acevedo JJ, Hernandez-Cruz A, Trevino CL. T-type Ca2+ channels in sperm function. Cell Calcium. 2006; 40:241-52.

[13] Eckle VS, Shcheglovitov A, Vitko I, Dey D, Yap CC, Winckler B, Perez-Reyes E. Mechanisms by which a CACNA1H mutation in epilepsy patients increases seizure susceptibility. J Physiol. 2014; 592:795-809.

[14] Elies J, Scragg JL, Boyle JP, Gamper N, Peers C. Regulation of the T-type Ca(2+) channel Cav3.2 by hydrogen sulfide: emerging controversies concerning the role of H2 S in nociception. J Physiol. 2016; 594:4119-29.

[15] Elies J, Scragg JL, Dallas ML, Huang D, Huang S, Boyle JP, Gamper N, Peers C. Inhibition of T-type Ca2+ Channels by Hydrogen Sulfide. Adv Exp Med Biol. 2015; 860:353-60.

[16] Elies J, Scragg JL, Huang S, Dallas ML, Huang D, MacDougall D, Boyle JP, Gamper N, Peers C. Hydrogen sulfide inhibits Cav3.2 T-type Ca2+ channels. FASEB J. 2014; 28:5376-87.

[17] Ernst WL, Zhang Y, Yoo JW, Ernst SJ, Noebels JL. Genetic enhancement of thalamocortical network activity by elevating alpha 1g-mediated low-voltage-activated calcium current induces pure absence epilepsy. J Neurosci. 2009; 29:1615-25.

[18] Ferdous Z, Qureshi MA, Jayaprakash P, Parekh K, John A, Oz M, Raza H, Dobrzynski H, Adrian TE, Howarth FC. Different Profile of mRNA Expression in Sinoatrial Node from Streptozotocin-Induced Diabetic Rat. PLoS One. 2016; 11:e0153934.

[19] Gadotti VM, Caballero AG, Berger ND, Gladding CM, Chen L, Pfeifer TA, Zamponi GW. Small organic molecule disruptors of Cav3.2 - USP5 interactions reverse inflammatory and neuropathic pain. Mol Pain. 2015; 11:12.

[20] Garcia-Caballero A, Gadotti VM, Chen L, Zamponi GW. A cell-permeant peptide corresponding to the cUBP domain of USP5 reverses inflammatory and neuropathic pain. Mol Pain. 2016; 12.

[21] Garcia-Caballero A, Gadotti VM, Stemkowski P, Weiss N, Souza IA, Hodgkinson V, Bladen C, Chen L, Hamid J, Pizzoccaro A, Deage M, Francois A, Bourinet E, Zamponi GW. The deubiquitinating enzyme USP5 modulates neuropathic and inflammatory pain by enhancing Cav3.2 channel activity. Neuron. 2014; 83:1144-58.

[22] Gilmore AJ, Heblinski M, Reynolds A, Kassiou M, Connor M. Inhibition of human recombinant T-type calcium channels by N-arachidonoyl 5-HT. Br J Pharmacol. 2012; 167:1076-88.

[23] Hayashi K, Wakino S, Sugano N, Ozawa Y, Homma K, Saruta T. Ca2+ channel subtypes and pharmacology in the kidney. Circ Res. 2007; 100:342-53.

[24] Heron SE, Khosravani H, Varela D, Bladen C, Williams TC, Newman MR, Scheffer IE, Berkovic SF, Mulley JC, Zamponi GW. Extended spectrum of idiopathic generalized epilepsies associated with CACNA1H functional variants. Ann Neurol. 2007; 62:560-8.

[25] Heron SE, Phillips HA, Mulley JC, Mazarib A, Neufeld MY, Berkovic SF, Scheffer IE. Genetic variation of CACNA1H in idiopathic generalized epilepsy. Ann Neurol. 2004; 55:595-6.

[26] Hu C, Depuy SD, Yao J, McIntire WE, Barrett PQ. Protein kinase A activity controls the regulation of T-type CaV3.2 channels by Gbetagamma dimers. J Biol Chem. 2009; 284:7465-73.

[27] Huang D, Huang S, Gao H, Liu Y, Qi J, Chen P, Wang C, Scragg JL, Vakurov A, Peers C, Du X, Zhang H, Gamper N. Redox-Dependent Modulation of T-Type Ca(2+) Channels in Sensory Neurons Contributes to Acute Anti-Nociceptive Effect of Substance P. Antioxid Redox Signal. 2016; 25:233-51.

[28] Huguenard JR. Low-voltage-activated (T-type) calcium-channel genes identified. Trends Neurosci. 1998; 21:451-2.
[29] Husse B, Franz WM. Generation of cardiac pacemaker cells by programming and differentiation. Biochim Biophys Acta. 2016; 1863:1948-52.
[30] Chemin J, Mezghrani A, Bidaud I, Dupasquier S, Marger F, Barrere C, Nargeot J, Lory P. Temperature-dependent modulation of CaV3 T-type calcium channels by protein kinases C and A in mammalian cells. J Biol Chem. 2007; 282:32710-8.
[31] Chemin J, Monteil A, Perez-Reyes E, Bourinet E, Nargeot J, Lory P. Specific contribution of human T-type calcium channel isotypes (alpha(1G), alpha(1H) and alpha(1I)) to neuronal excitability. J Physiol. 2002; 540:3-14.
[32] Chemin J, Monteil A, Perez-Reyes E, Nargeot J, Lory P. Direct inhibition of T-type calcium channels by the endogenous cannabinoid anandamide. EMBO J. 2001; 20:7033-40.
[33] Chen Y, Lu J, Pan H, Zhang Y, Wu H, Xu K, Liu X, Jiang Y, Bao X, Yao Z, Ding K, Lo WH, Qiang B, Chan P, Shen Y, Wu X. Association between genetic variation of CACNA1H and childhood absence epilepsy. Ann Neurol. 2003; 54:239-43.
[34] Kang HW, Park JY, Jeong SW, Kim JA, Moon HJ, Perez-Reyes E, Lee JH. A molecular determinant of nickel inhibition in $Ca_v3.2$ T-type calcium channels. J Biol Chem. 2006; 281:4823-30.
[35] Kawabata A, Ishiki T, Nagasawa K, Yoshida S, Maeda Y, Takahashi T, Sekiguchi F, Wada T, Ichida S, Nishikawa H. Hydrogen sulfide as a novel nociceptive messenger. Pain. 2007; 132:74-81.
[36] Kim D, Song I, Keum S, Lee T, Jeong MJ, Kim SS, McEnery MW, Shin HS. Lack of the burst firing of thalamocortical relay neurons and resistance to absence seizures in mice lacking a_{1G} T-type Ca^{2+} channels. Neuron. 2001; 31:35-45.
[37] Lacinova L. Pharmacology of recombinant low-voltage activated calcium channels. Curr Drug Targets CNS Neurol Disord. 2004; 3:105-11.
[38] Lacinova L. Voltage-dependent calcium channels. Gen Physiol Biophys. 2005; 24 Suppl 1:1-78.
[39] Lacinova L, Klugbauer N, Hofmann F. Low voltage activated calcium channels: from genes to function. Gen Physiol Biophys. 2000; 19:121-36.
[40] Lalevee N, Rebsamen MC, Barrere-Lemaire S, Perrier E, Nargeot J, Benitah JP, Rossier MF. Aldosterone increases T-type calcium channel expression and in vitro beating frequency in neonatal rat cardiomyocytes. Cardiovasc Res. 2005; 67:216-24.
[41] Lazniewska J, Rzhepetskyy Y, Zhang FX, Zamponi GW, Weiss N. Cooperative roles of glucose and asparagine-linked glycosylation in T-type calcium channel expression. Pflugers Arch. 2016.
[42] Li L, Rose P, Moore PK. Hydrogen sulfide and cell signaling. Annu Rev Pharmacol Toxicol. 2011; 51:169-87.
[43] M'Dahoma S, Gadotti VM, Zhang FX, Park B, Nam JH, Onnis V, Balboni G, Lee JY, Zamponi GW. Effect of the T-type channel blocker KYS-05090S in mouse models of acute and neuropathic pain. Pflugers Arch. 2016; 468:193-9.
[44] Maturana A, Lenglet S, Python M, Kuroda S, Rossier MF. Role of the T-type calcium channel CaV3.2 in the chronotropic action of corticosteroids in isolated rat ventricular myocytes. Endocrinology. 2009; 150:3726-34.
[45] Monteil A, Chemin J, Leuranguer V, Altier C, Mennessier G, Bourinet E, Lory P, Nargeot J. Specific properties of T-type calcium channels generated by the human a_{1I} subunit. J Biol Chem. 2000; 275:16530-5.
[46] Moremen KW, Tiemeyer M, Nairn AV. Vertebrate protein glycosylation: diversity, synthesis and function. Nat Rev Mol Cell Biol. 2012; 13:448-62.
[47] Nelson MT, Woo J, Kang HW, Vitko I, Barrett PQ, Perez-Reyes E, Lee JH, Shin HS, Todorovic SM. Reducing agents sensitize C-type nociceptors by relieving high-affinity zinc inhibition of T-type calcium channels. Journal of Neuroscience. 2007; 27:8250-8260.
[48] Ohkubo T, Inoue Y, Kawarabayashi T, Kitamura K. Identification and electrophysiological characteristics of isoforms of T-type calcium channel Ca(v)3.2 expressed in pregnant human uterus. Cell Physiol Biochem. 2005; 16:245-54.
[49] Ondacova K, Karmazinova M, Lazniewska J, Weiss N, Lacinova L. Modulation of Cav3.2 T-type calcium channel permeability by asparagine-linked glycosylation. Channels (Austin). 2016; 10:175-84.
[50] Orestes P, Osuru HP, McIntire WE, Jacus MO, Salajegheh R, Jagodic MM, Choe W, Lee J, Lee SS, Rose KE, Poiro N, Digruccio MR, Krishnan K, Covey DF, Lee JH, Barrett PQ, Jevtovic-Todorovic V, Todorovic SM. Reversal of neuropathic pain in diabetes by targeting glycosylation of Ca(V)3.2 T-type calcium channels. Diabetes. 2013; 62:3828-38.
[51] Perez-Reyes E. Molecular physiology of low-voltage-activated T-type calcium channels. Physiol Rev. 2003; 83:117-61.
[52] Ross HR, Gilmore AJ, Connor M. Inhibition of human recombinant T-type calcium channels by the endocannabinoid N-arachidonoyl dopamine. Br J Pharmacol. 2009; 156:740-50.
[53] Rzhepetskyy Y, Lazniewska J, Blesneac I, Pamphlett R, Weiss N. CACNA1H missense mutations associated with amyotrophic lateral sclerosis alter Cav3.2 T-type calcium channel activity and reticular thalamic neuron firing. Channels (Austin). 2016; 10:466-77.
[54] Scholl UI, Stolting G, Nelson-Williams C, Vichot AA, Choi M, Loring E, Prasad ML, Goh G, Carling T, Juhlin CC, Quack I, Rump LC, Thiel A, Lande M, Frazier BG, Rasoulpour M, Bowlin DL, Sethna CB, Trachtman H, Fahlke C, Lifton RP. Recurrent gain of function mutation in calcium channel CACNA1H causes early-onset hypertension with primary aldosteronism. Elife. 2015; 4:e06315.
[55] Splawski I, Timothy KW, Decher N, Kumar P, Sachse FB, Beggs AH, Sanguinetti MC, Keating MT. Severe arrhythmia disorder caused by cardiac L-type calcium channel mutations. Proc Natl Acad Sci U S A. 2005; 102:8089-96; discussion 8086-8.
[56] Splawski I, Timothy KW, Sharpe LM, Decher N, Kumar P, Bloise R, Napolitano C, Schwartz PJ, Joseph RM, Condouris K, Tager-Flusberg H, Priori SG, Sanguinetti MC, Keating MT. Ca(V)1.2 calcium channel dysfunction causes a multisystem disorder including arrhythmia and autism. Cell. 2004; 119:19-31.
[57] Splawski I, Yoo DS, Stotz SC, Cherry A, Clapham DE, Keating MT. CACNA1H mutations in autism spectrum disorders. J Biol Chem. 2006; 281:22085-91.
[58] Steinberg KM, Yu B, Koboldt DC, Mardis ER, Pamphlett R. Exome sequencing of case-unaffected-parents trios reveals recessive

and de novo genetic variants in sporadic ALS. Sci Rep. 2015; 5:9124.

[59] Todorovic SM, Jevtovic-Todorovic V. Neuropathic pain: role for presynaptic T-type channels in nociceptive signaling. Pflugers Arch. 2013; 465:921-7.

[60] Ufret-Vincenty CA, Baro DJ, Lederer WJ, Rockman HA, Quinones LE, Santana LF. Role of sodium channel deglycosylation in the genesis of cardiac arrhythmias in heart failure. J Biol Chem. 2001; 276:28197-203.

[61] Wang G, Bochorishvili G, Chen Y, Salvati KA, Zhang P, Dubel SJ, Perez-Reyes E, Snutch TP, Stornetta RL, Deisseroth K, Erisir A, Todorovic SM, Luo JH, Kapur J, Beenhakker MP, Zhu JJ. CaV3.2 calcium channels control NMDA receptor-mediated transmission: a new mechanism for absence epilepsy. Genes Dev. 2015; 29:1535-51.

[62] Watanabe I, Wang HG, Sutachan JJ, Zhu J, Recio-Pinto E, Thornhill WB. Glycosylation affects rat Kv1.1 potassium channel gating by a combined surface potential and cooperative subunit interaction mechanism. J Physiol. 2003; 550:51-66.

[63] Weiss N, Black SA, Bladen C, Chen L, Zamponi GW. Surface expression and function of Cav3.2 T-type calcium channels are controlled by asparagine-linked glycosylation. Pflugers Arch. 2013; 465:1159-70.

[64] Welsby PJ, Wang H, Wolfe JT, Colbran RJ, Johnson ML, Barrett PQ. A mechanism for the direct regulation of T-type calcium channels by Ca2+/calmodulin-dependent kinase II. J Neurosci. 2003; 23:10116-21.

[65] Yao J, Davies LA, Howard JD, Adney SK, Welsby PJ, Howell N, Carey RM, Colbran RJ, Barrett PQ. Molecular basis for the modulation of native T-type Ca2+ channels in vivo by Ca2+/calmodulin-dependent protein kinase II. J Clin Invest. 2006; 116:2403-12.

[66] Zamponi GW, Striessnig J, Koschak A, Dolphin AC. The Physiology, Pathology, and Pharmacology of Voltage-Gated Calcium Channels and Their Future Therapeutic Potential. Pharmacol Rev. 2015; 67:821-70.

[67] Zhang Y, Cribbs LL, Satin J. Arachidonic acid modulation of alpha1H, a cloned human T-type calcium channel. Am J Physiol Heart Circ Physiol. 2000; 278:H184-93.

[68] Zoghbi HY. Postnatal neurodevelopmental disorders: meeting at the synapse? Science. 2003; 302:826-30.

DE GRUYTER OPEN

Eur. Pharm. J. 2017, 64 (2): 22-23.
ISSN 1338-6786 (online) and ISSN 2453-6725 (print version),
DOI: 10.1515/afpuc-2016-0015

EUROPEAN PHARMACEUTICAL JOURNAL

Mechanical properties of lipid bilayers

Short Paper

Nagle JF.✉

Carnegie Mellon University,
Department of Physics
Pittsburgh, USA

Received 15 September, 2016, accepted 24 October, 2016

Keywords *Bending modulus – Tilt modulus – x-ray scattering*

I. INTRODUCTION

Everyone agrees that the bending modulus (also known as K_C or κ) is an important property of biomembranes, as it quantifies the flexibility that is important to cell functions (Nagle, 2013). For many years, we have used the traditional Canham–Helfrich model for fluctuations to analyse diffuse X-ray scattering in order to obtain values for the bending modulus K_C (Liu & Nagle, 2004). Theory and molecular dynamics simulations have suggested that the next level of refinement to describe membrane fluctuations should extend this model to include molecular tilting (May et al., 2007). This extension is widely considered to be important for understanding membrane fusion (Ryham et al., 2016). Of the two versions of an extended model, the Brown model (Watson et al., 2011) has been shown to provide the more accurate description of the hydrocarbon chains as determined by simulations (Kopelevich & Nagle, 2015).

II. EXPERIMENTAL

Our primary experimental technique is X-ray scattering from stacks of fully hydrated lipid bilayers. In addition to the usual quasi-Bragg peaks, these samples exhibit extensive diffuse scattering that contains more information than the peaks. In particular, we have been obtaining the bending modulus K_C from diffuse scattering, which is one focus of this talk. Quantities also obtained that were not focused on are the electron density profile and the bulk B modulus that is a measure of interactions between neighbouring bilayers in the stack. Recently, we have learned how to include molecular tilt in our analysis of X-ray data. We found that the X-ray data are fit better for the tilt-dependent model, and we have reported the first experimental value of the tilt modulus K_θ for dioleoylphosphatidylcholine lipid bilayers (Jablin et al., 2014). This has required considerable theoretical, analytical and software development (Jablin, 2015). Re-analysis that includes the tilt modulus is now being performed on extensive earlier X-ray scattering data collected in my laboratory.

III. RESULTS AND DISCUSSION

Preliminary results for the tilt modulus of dimyristoylphosphatidylcholine (DMPC) were shown. It is noteworthy that two recent atomistic simulations (Venable et al., 2015; Wang & Deserno, 2016) each performed at only one temperature, agree well with our experimental results. However, my most striking result, not yet investigated by simulations, is the rapid decrease in K_θ as the main transition in DMPC is approached by lowering the temperature within the fluid phase. This provides a new perspective for the DMPC main phase transition. In critical phenomena, the vanishing of the modulus corresponding to an order parameter results in spontaneous symmetry breaking of that order parameter. It is well known that there is spontaneous tilt in the gel phase. Although the main transition is into the ripple phase that is complicated by ripple symmetry breaking, recent structural work (Akabori & Nagle, 2015) shows that the ripple phase also

* *E-mail: nagle@cmu.edu*

has spontaneous tilt (along with other interesting features not comprehended by existing theory). This supports the previous interpretation that there is pre-critical behaviour above the transition, as originally evidenced by the accelerating decrease in volume on approach to the transition (Nagle & Wilkinson, 1978). However, whilst tilt acts like an order parameter with spontaneous symmetry breaking at the transition, there is clearly much more going on, and area/lipid is probably the most important order parameter (Nagle, 1986) and a full theory should probably also include the spontaneous symmetry breaking of rippling in the ripple phase.

The new tilt-dependent analysis continues to find that K_C also decreases as the main transition is approached from the fluid phase (Chu et al., 2005). The decrease now begins at a lower temperature (27 °C) than the previous one (30 °C), above which K_C decreases with increasing temperature. The new maximum agrees better with the onset of the anomalous swelling regime.

The older tilt-independent analysis essentially assumed that the tilt modulus was infinite. Allowing a finite tilt modulus in the analysis of a data set increases the obtained value of K_C.

Values of the bending modulus K_C from the new tilt-dependent analysis were compared to those obtained by the classical methods that use giant unilamellar vesicles. Compared to what has been discussed previously (Nagle, 2013) this reduces the differences between the X-ray values of K_C and the generally larger values obtained by other experimental methods that sense membrane flexibility on much larger length scales than the X-ray method and that are, therefore, insensitive to tilt (Nagle et al., 2015). Nevertheless, there are still outstanding discrepancies in the values of the bending modulus that might have been due to the effect of sugar used at different concentrations in the classical experiments. However, we have been unable to find the effect of sugars in our experiments (Nagle et al., 2016).

ACKNOWLEDGEMENT

I thank the 4th European Joint Theoretical/Experimental Meeting on Membranes (7–9 September, 2016, in Bratislava, Slovakia) and its organisers for sponsoring my travel.

References

[1] Akabori K, Nagle JF. Structure of the DMPC lipid bilayer ripple phase. Soft Matter 2015; 11:918-926.
[2] Chu N, Kucerka N, Liu YF, Tristram-Nagle S, Nagle JF. Anomalous swelling of lipid bilayer stacks is caused by softening of the bending modulus. Phys Rev E. 2005; 71:041904(1-8).
[3] Jablin MS, Akabori K, Nagle JF. Experimental Support for Tilt-Dependent Theory of Biomembrane Mechanics. Phys Rev Lett. 2014;113: 248102 (1-5).
[4] Jablin, M. S., Tilt-Dependent Analysis of Diffuse X-ray Scattering from Oriented Stacks of fluid Phase Lipid Bilayers. Thesis: http://lipid.phys.cmu.edu, 2015; pp. 1-257.
[5] Kopelevich DI, Nagle JF. Correlation between length and tilt of lipid tails. J Chem Phys. 2015; 143:154702(1-8).
[6] Liu YF, Nagle JF. Diffuse scattering provides material parameters and electron density profiles of biomembranes. Phys Rev E. 2004;69:040901(1-4).
[7] May ER, Narang A, Kopelevich DI. Role of molecular tilt in thermal fluctuations of lipid membranes. Phys Rev E. 2007;76:021913(1-6).
[8] Nagle JF. Introductory Lecture: Basic quantities in model biomembranes. Faraday Discuss. 2013;161:11-29.
[9] Nagle JF, Wilkinson DA. Lecithin Bilayers - Density-Measurements and Molecular-Interactions. Biophys J. 1978;23:159-175.
[10] Nagle JF. Theory of Lipid Monolayer and Bilayer Chain-Melting Phase-Transitions. Faraday Discuss. 1986;81:151-162.
[11] Nagle JF, Jablin MS, Tristram-Nagle S, Akabori K. What are the true values of the bending modulus of simple lipid bilayers? Chem Phys Lipids. 2015;185:3-10.
[12] Nagle JF, Jablin MS, Tristram-Nagle S. Sugar does not affect the bending and tilt moduli of simple lipid bilayers. Chem Phys Lipids. 2016;196:76-80.
[13] Ryham RJ, Klotz TS, Yao LH, Cohen F S. Calculating Transition Energy Barriers and Characterizing Activation States for Steps of Fusion. Biophys J. 2016;110:1110-1124.
[14] Venable RM, Brown FLH, Pastor RW. Mechanical properties of lipid bilayers from molecular dynamics simulation. Chem Phys Lipids. 2015;192:60-67.
[15] Wang X, Deserno M. Determining the Lipid Tilt Modulus by Simulating Membrane Buckles. J Phys Chem B. 2016;120:6061-6073.
[16] Watson MC, Penev ES, Welch PM, Brown FLH. Thermal fluctuations in shape, thickness, and molecular orientation in lipid bilayers. J Chem Phys. 2011;135:(1-22).

DE GRUYTER OPEN

Eur. Pharm. J. 2017, 64 (2): 24-27.
ISSN 1338-6786 (online) and ISSN 2453-6725 (print version),
DOI: 10.1515/afpuc-2017-0003

EUROPEAN PHARMACEUTICAL JOURNAL

Effect of urea and tmao on lipid bilayers

Original Paper

Valerio J.[1], Bernstorff S.[2], Funari S.S.[1]✉

[1]*Photo Science at DESY, Hamburg, Germany*
[2]*Elettra-Sincrotrone Trieste S.C.p.A, Trieste, Italy*

Received 1 November, 2016, accepted 16 March, 2017

Abstract We study the effect of the osmolytes, Urea and trimethylamine-N-oxide (TMAO) on POPE (1-palmitoyl-2-oleoyl-*sn*-glycero-3-phosphoethanolamine) lipid membranes using SAXS/WAXS and DSC. Their antagonist effect is observed with TMAO stabilizing and Urea destabilizing the lipid bilayer, as seen by others in earlier researches.

Keywords *lipid membranes – phase transitions – osmocytes – X-rays – DSC*

INTRODUCTION

Lipid bilayers display a wide range of morphologies (di Vitta *et al.*, 2013; Funari *et al.,* 2009, 2011; Silva *et al.,* 2013; Valerio *et al.,* 2012) and are simple models for the cell membrane. They not only provide a matrix for anchoring a variety of substances, for example, membrane proteins, glycolipids and so on, that play an essential role in the cell metabolism, but also define the cell limits keeping apart the inner and outer environments. Recently, we studied the structural effects of synthetic quinones on lipid model membranes in order to investigate their contribution to morphologies, possibly involved in transfer processes. Summarizing, we can say that the insertion of these additives lowers the temperature of the structural phase transitions, and in many cases, induce the formation of cubic phases at low temperatures,[1, 2] which corresponds to an increase in the lipid matrix surface curvature.

It is accepted that urea and (TMAO) have antagonistic effects on the fluidity of lipid membranes (Barton *et al.,* 1998; Meersman & Walsh, 2011; Seibel *et al.,* 2002). In red blood cells, urea slightly increases the gel-phase domains, but this effect is counteracted by TMAO. We intend to determine how these solutes affect the lipid membrane and determine their contribution to fluidity, or curvature, induced on them.

OBJECTIVES

We intended to study the influence of natural osmolytes urea and TMAO on the fluidity and stability of lipid model membranes by determining the structure of the phases formed in the lipid dispersions. In this way, we expect to determine whether a dominant interaction of these solutes takes place on the lipids, or more indirectly, by affecting the properties of the aqueous region near the headgroup surface. Small and wide angle X-ray scattering (SAXS/WAXS) thermal scans enable us to determine the number of phases in each system, their transitions and respective reversibility. SAXS/WAXS identifies these structures and provide the dimensions of their lattices. Differential scanning calorimetry (DSC) provides the phase transition temperatures and the respective energy involved in such processes.

MATERIALS AND METHODS

The samples were prepared by mixing desired volumes of stock solutions with well-defined concentrations of its components. The aqueous media at a temperature above the lipid main phase transition was directly added to the lipid. The samples were agitated slowly for two hours before they were filled into glass capillaries of 1.5 mm diameter and sealed. All chemicals were commercially available in high purity (POPE: Avanti lipids, TMAO and UREA : Sigma) and used without further purification.

At the SAXS beamline of ELETTRA, an in-line micro-calorimeter built by the group of Michel Ollivon (CNRS, Paris, France) (M. Ollivon *et al.*, 2006) was used to simultaneously

* *E-mail: sergio.funari@desy.de*

measure SAXS/WAXD and high sensitivity DSC from the same sample. The calorimeter was programed to heat and cool the sample with a rate of 1°C/min during the thermal scans between 15 and 85°C. The acquisition time was 5 s each minute, and monochromatic synchrotron radiation of 0.154 nm wavelength was used. SAXS was monitored with a bi-dimensional Pilatus 1M detector positioned *ca.* 1 m away from the sample. WAXS was measured with a Pilatus 100 K detector at a sample to detector distance of ca. 15 cm.

RESULTS AND DISCUSSION

Thermal scans on lipid matrices prepared with aqueous solutions of Urea or TMAO have shown morphologies similar to the ones observed in aqueous solution of the pure lipids, although with different dimensions and transition temperatures. In POPE, we observe structures with high curvature, and upon temperature cycling, the induction of cubic phases (see Figure 1), whose structure could not be uniquely identified due to the lack of resolution or a significant number of diffraction peaks originating from the samples. We note the absence of independent SAXS-based data available in the literature for the structural effect of such solutes. Some salts favour the formation of cubic phases in POPE, as described elsewhere (Tenchov & Koynova, 2012).

A fully hydrated sample prepared in 400 mM TMAO shows the expected transitions normally seen in POPE. However, surprisingly there is a significant absence of diffraction over a wide range of temperatures on cooling from the hexagonal phase, and the diffraction peaks in the last patterns have a much lower intensity as compared to the ones at the beginning of the scan, as shown in fig 2. The DSC traces on heating and cooling indicate phase transitions on heating at temperatures higher than for pure aqueous POPE, while during cooling this is not seen (Figure 3). We note that some signals were too weak and therefore not subject to our in-depth interpretation. The high temperatures of the phase transition on heating indicate a stabilization of the phases.

Together with the observation that some samples have an 'oily' appearance, we conclude that TMAO hinders the self-assembly of such lipid once it interacts, most likely via hydrogen bonds, with the PE head groups. The interactions seem to become more effective at high temperatures and do not vanish easily or fast enough at our time scale during cooling. This finds support in the study on '*Hydrophobic association in mixed urea-TMAO solutions*' by Ganguly et al. (2016).

Urea 200mM has a milder effect on the POPE dispersion, see fig 4. The DSC trace shows a transition at a temperature higher than for pure POPE and POPE in 400 mM TMAO, however involving less heat than the previous system. The thermal SAXS scan indicates a less organized stack of bilayers. The hexagonal phase, normally following the lamellar upon heating, could not be seen up to the highest temperatures of 85°C. Moreover, no organized structure was formed during the whole temperature range during cooling. This is clear evidence that Urea has a destabilizing effect on the formed structures due to the interaction on the headgroup interface region of the bilayers assembly.

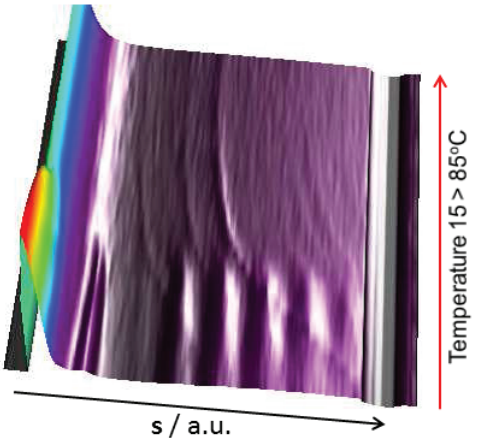

Figure1 . Heating SAXS scan (15 -> 85 oC) of a POPE dispersion in solution of TMAO:Urea (2:1). The sample has been through 5 temperature cycles before this measurement. We note the occurrence of several peaks at very low angles (below the known peak of the lamellar phase). Near the beam stop (left) one sees other peaks very close to each other whose interpretation is still unclear at this point.

CONCLUSIONS

On combining SAXS/WAXS and DSC results obtained from dispersions of POPE in either aqueous solution of TMAO or Urea, one can see their antagonistic effect from a structural perspective, that is, their influence on the macro organization of the self-assembled mesogenic units.

Both osmolytes seem to require high temperatures (or weaker interactions between headgroups of neighbouring lipids) to be able to effectively interact with the POPE (headgroups) and exert their influence on the organization of the dispersion. TMAO favours the lamellar layer structures, while urea tends to hinder the macro organization of the system.

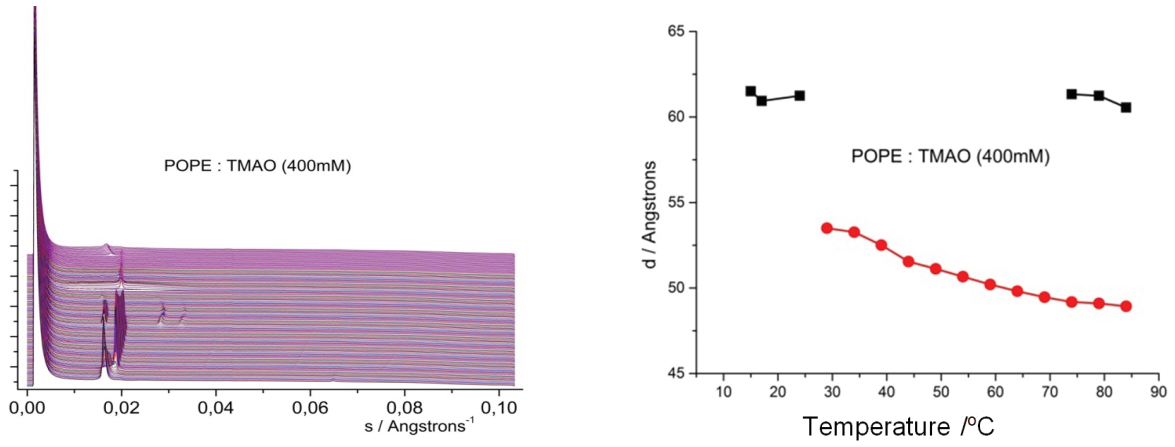

Figure 2. Sequence of diffraction patterns of POPE/TMAO. Left: Temperature scan from 15 -> 85 -> 15oC. Right: Measured spacings (thermal evolution upon heating), d.

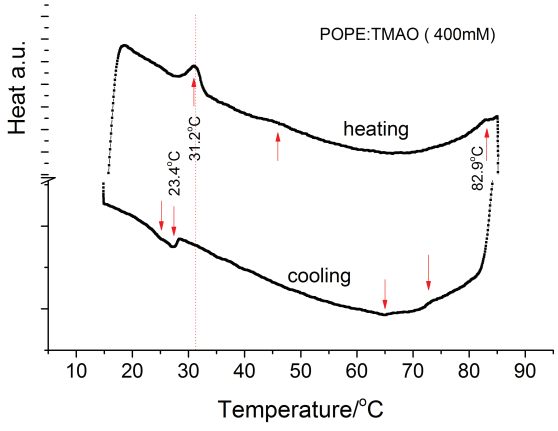

Figure 3. DSC trace of a dispersion of POPE in 400 mM TMAO. The arrows indicate phase transition signals, many too faint to be considered for in-depth analysis.

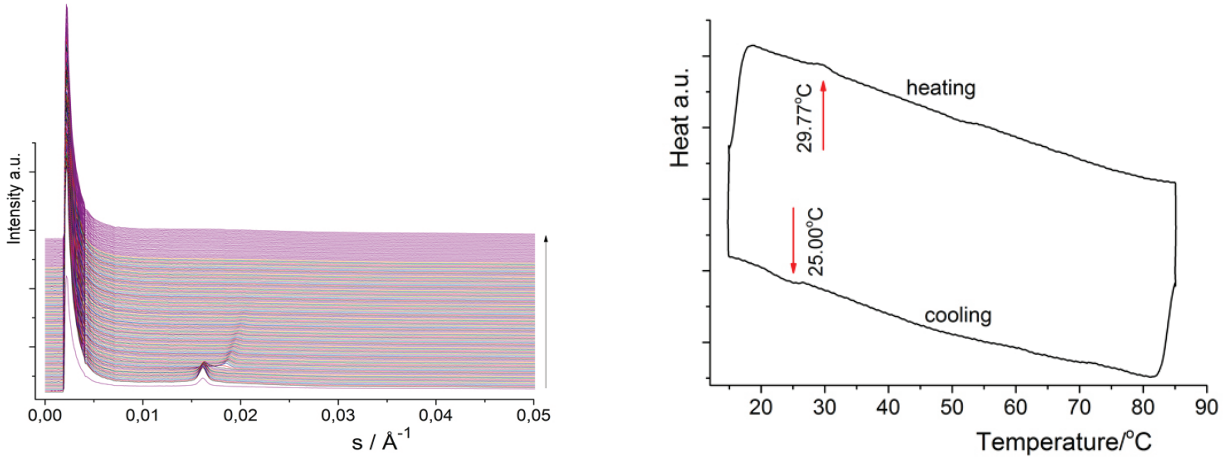

Figure 4. Thermal SAXS scan of a POPE:Urea 200mM dispersion (left) and the corresponding DSC trace (right).

References

[1] Di Vitta C, Marzorati L, Funari SS. Modification of Phospholipid Bilayers Induced by Sulfurated Naphthoquinones. J. Lipids, 2013, Article ID 592318.

[2] Funari SS, Rebbin V, Marzorati L, Di Vitta C. Membrane morphology modifications induced by hydroquinones. Langmuir, 2011, **27** (13), 8257-8262.

[3] Funari SS, Rapp G, Richter F. Double-bilayer: a new phase formed by lysophospholipids and the corresponding fatty acid. Quim. Nova, 2009, **32**(4), 908-912.

[4] Valerio J, Lameiro HM; Funari SS, Moreno MJ, Eurico E.Temperature Effect on the Bilayer Stacking in Multilamellar Lipid Vesicles. J. Phys Chem. B, 2012, **11**6(1), 168-178.

[5] Silva T, Adao R, Nazmi K, Bolscher JGM, Funari SS, Uhrikova D, Bastos M. Structural diversity and mode of action on lipid membranes of three lactoferrin candidacidal peptides. Biochim Biophys Acta, 2013, **1828**(11), 2796-2796.

[6] Barton KN, Buhr MM, Ballantyne J.S. Effects of urea and trimethylamine N-oxide on fluidity of liposomes and membranes of an elasmobranch; Am. J. Physiol.-Regulat. Integ. Comp. Physiol. 1998, **276**, R397–R406.

[7] Seibel BA, Walsh PJ. Trimethylamine oxide accumulation in marine animals: relationship to acylglycerol storage. J. Exp. Biol. 2002, **198**, 373–378.

[8] Meersman F, Bowron D, Soper AK, Koch MHJ. An X-ray and neutron scattering study of the equilibrium between trimethylamine N-oxide and urea in aqueous solution. Phys. Chem. Chem. Phys.2011, **13**(30), 13765-13771.

[9] Tenchov B & Koynova R. Cubic phases in membrane lipids**.** Eur Biophys J (2012),41:841.

[10] Ganguly P, van der Vergt NFA Shea JE. Hydrophobic association in mixed urea-TMAO solutions, J. Phys. Chem. Let. 2016, **7**(15), 3052-3069.

[11] Ollivon M, Keller G, Bourgaux C, Kalnin D, Villeneuve P, Lesieur P., J. Therm Anal Calorim; DSC and high resolution X-ray diffraction coupling ; Therm. Anal. Calorim. 2006, **85**(1), 219 .

DE GRUYTER OPEN

Eur. Pharm. J. 2017, 64 (2): 28-35.
ISSN 1338-6786 (online) and ISSN 2453-6725 (print version),
DOI: 10.1515/afpuc-2017-0004

EUROPEAN PHARMACEUTICAL JOURNAL

Ceramides in the skin barrier

Original Paper

Vávrová K.,✉ Kováčik A., Opálka L.

Charles University, Faculty of Pharmacy in Hradec Králové, Skin Barrier Research Group, Hradec Králové, Czech Republic

Received 31 October, 2016, accepted 7 December, 2016

Abstract The skin barrier, which is essential for human survival on dry land, is located in the uppermost skin layer, the stratum corneum. The stratum corneum consists of corneocytes surrounded by multilamellar lipid membranes that prevent excessive water loss from the body and entrance of undesired substances from the environment. To ensure this protective function, the composition and organization of the lipid membranes is highly specialized. The major skin barrier lipids are ceramides, fatty acids and cholesterol in an approximately equimolar ratio. With hundreds of molecular species of ceramide, skin barrier lipids are a highly complex mixture that complicate the investigation of its behaviour. In this minireview, the structures of the major skin barrier lipids, formation of the stratum corneum lipid membranes and their molecular organization are described.

Keywords *Skin barrier – stratum corneum – ceramide – sphingolipid*

FUNDING

This work was supported by the Czech Science Foundation – German Science Foundation joint project 16-25687J.

INTRODUCTION

Ceramides, that is, *N*-acylsphingosines belong to the family of sphingolipids. Ceramides regulate several cellular processes, such as proliferation, differentiation and apoptosis (Hannun, 1996; Hannun and Obeid, 2008). In human body, ceramides are equally important outside the cell – they form multilamellar lipid membranes between corneocytes of the uppermost skin layer, the stratum corneum (Candi et al., 2005). These stratum corneum lipids prevent excessive water loss from the body and hamper the penetration of undesired substances, allergens and microbes from the environment into the body (Bouwstra and Ponec, 2006; Elias, 2008). In fact, the development of such lipid-based barrier was an essential step in the evolution of life on dry land. In this minireview, the structures of major skin barrier lipids, formation of the stratum corneum lipid membranes and their molecular organization are described.

COMPOSITION OF THE SKIN LIPID BARRIER

Human stratum corneum is composed of approximately 15–25 layers of flattened dead cells, corneocytes, which are surrounded by a lipid matrix (Elias et al., 1977). To provide a competent barrier function, the lipids in the stratum corneum are highly specialized: there are virtually no phospholipids; the major constituents are ceramides, free fatty acids and cholesterol in an approximately 1:1:1 molar ratio (**Fig. 1**). This equimolar ratio seems to be highly important for epidermal homeostasis, as alterations in this lipid composition were associated with a disturbed barrier function (Breiden and Sandhoff, 2014; Feingold and Elias, 2014; Holleran et al., 2006; Rabionet et al., 2014; van Smeden et al., 2014b).

Free fatty acids in the skin barrier are 14–34 carbons long, mostly saturated and unbranched. The predominant fatty acids have 24 carbons (lignoceric acid) and 26 carbons (cerotic acid) – these two species comprise approximately 50 weight % of the stratum corneum fatty acids (Norlen et al., 1998; van Smeden et al., 2014a). Unsaturated and shorter fatty acids are present in the stratum corneum lipid membranes only in minor quantities; their concentrations increase in pathological conditions such as atopic dermatitis, probably due to filaggrin

* *E-mail: katerina.vavrova@faf.cuni.cz*

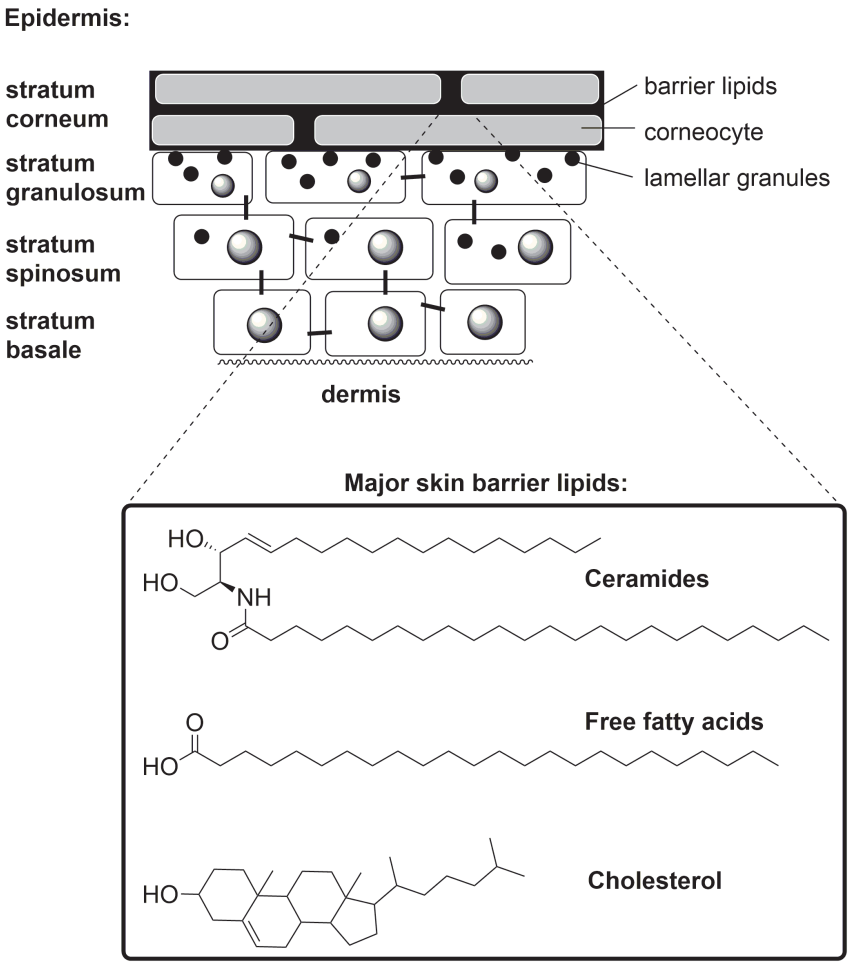

Figure 1. Schematic representation of epidermal layers, structure of the stratum corneum and the major skin barrier lipids.

deficiency (Jakasa et al., 2011; Jungersted et al., 2010; Vavrova et al., 2014).

Cholesterol is the main sterol in the skin lipid barrier. Cholesterol is also essential for the correct skin barrier function; it contributes to the correct lamellar and lateral structure and lipid fluidity (Feingold and Elias, 2014; Mojumdar et al., 2015a). Previous studies described separation of cholesterol from the lamellar phases (Mojumdar et al., 2015b; Schreiner et al., 2000); however, the physiological relevance of this separation is not known. In contrast, recent study using very high resolution electron microscopy on vitreous skin sections found no cholesterol crystals (Iwai et al., 2012).

Cholesteryl sulphate, that is, ester of sulphuric acid with cholesterol, is a minor component of the stratum corneum lipid matrix; it is present in approximately 5% of the barrier lipids (or approximately 2% of all lipids including surface lipids (Lampe et al., 1983)). The role of cholesteryl sulphate is probably not fully understood, one possible function of this molecule is that it contributes to the stratum corneum cohesion and regulates desquamation (Long et al., 1985).

CHEMISTRY OF CERAMIDES

The dominant lipids in the stratum corneum are ceramides; they constitute approximately one third of lipid molecules or 50% of the lipids by weight (van Smeden et al., 2014b). These simple sphingolipids have a relatively small polar head that does not extensively hydrate and two hydrophobic chains – the sphingoid base chain and *N*-acyl chain (fatty acid chain). The most intriguing fact in skin ceramides is their heterogeneity: 15 ceramide subclasses have been described until the present and together with the different chain lengths, this yields hundreds of distinct chemical structures (**Fig. 2**). For a recent review, see (Rabionet et al., 2014).

All ceramides are based on a sphingoid base, which is a long chain (usually 18 carbons) amino alcohol. The skin ceramides can contain sphingosine (S) and dihydrosphingosine (dS), which are common in eukaryotic cells, phytosphingosine (P), which is found only in some human tissues, and 6-hydroxysphingosine (H), which is specific for the epidermis (Kováčik et al., 2014). Recently, a novel tetrahydroxylated sphingoid base, which

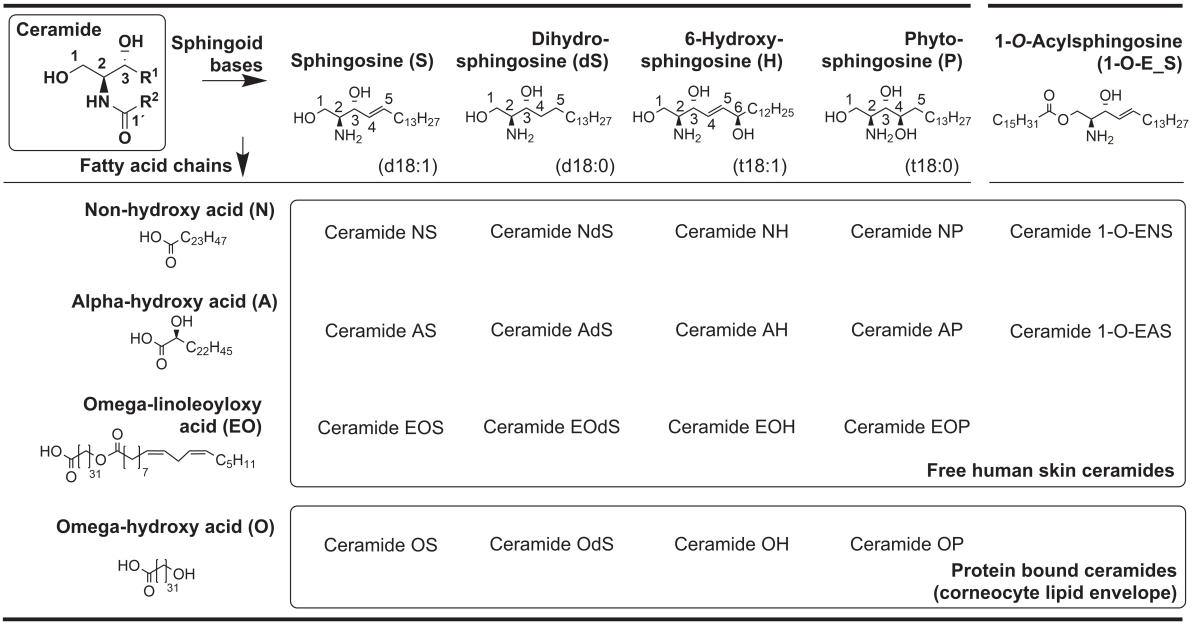

Figure 2. Chemical structures of the main components of the stratum corneum ceramides and their shorthand nomenclature.

has not been fully structurally described, has been found (t'Kindt et al., 2012). In ceramides, the primary amino group of the sphingoid base is acylated (that is, amide-linked) with a fatty acid, which is usually saturated, unbranched and very long (approximately 24 carbons) or ultralong (up to 38 carbons, mostly 30–32 carbons) (Breiden and Sandhoff, 2014; van Smeden et al., 2011). The fatty acid chain in ceramides can be without further substitution (N), α-hydroxylated (A) or, in case of ultralong chains, ω-hydroxylated (O) (Breiden and Sandhoff, 2014; Novotný et al., 2010; Rabionet et al., 2014; van Smeden et al., 2014b). The ω-hydroxyl is further ester-bound either to linoleic acid (EO) or to glutamate residues of the proteins (mostly involucrin) at the surface of a corneocyte (Candi et al., 2005). Recently, a new class of ceramides with three hydrophobic chains was discovered with the third chain ester-linked to the primary hydroxyl in position 1 of the sphingoid base (1-O-E) (Rabionet et al., 2013).

The letters in parentheses refer to the shorthand nomenclature developed by Motta (Motta et al., 1993) and expanded by Robson (Robson et al., 1994), Masukawa (Masukawa et al., 2008) and Rabionet (Rabionet et al., 2014). The ceramide structure is defined by a combination of the above-mentioned letters that specify the acyl with letters for the sphingoid part (**Fig. 2**). Thus, for example, *N*-lignoceroylsphingosine is ceramide NS or, more precisely, ceramide NS24, where the number 24 defines the fatty acid chain length.

FORMATION OF THE SKIN LIPID BARRIER; CORNEOCYTE LIPID ENVELOPE

The skin lipids are synthesized in the epidermal cells, keratinocytes, converted to their more polar precursors (e.g., ceramides are converted to sphingomyelins and glucosylceramides) (Holleran et al., 2006; Jensen et al., 1999), which are stored in lamellar granules together with catabolic enzymes. At the stratum granulosum/stratum corneum interface, the lamellar granules migrate to the keratinocyte upper surface, merge with plasma membrane, and secrete their contents into the intercellular space. The enzymes are activated and convert lipid precursors to barrier lipids that eventually assemble into lamellar structures that fill the entire space between the cells (Mizutani et al., 2009; Rabionet et al., 2014; Uchida and Holleran, 2008).

Some of the glucosylceramides of the EO-subclass, or acylglucosylceramides, are oxidized at their linoleic acid tail, which is then removed and the remaining ω-hydroxyceramides are attached via their ω-hydroxyl to glutamate residues of the corneocyte proteins involucrin and loricrin (Banks-Schlegel and Green, 1981; Behne et al., 2000). These covalent lipid monolayer, the corneocyte lipid envelope (Elias et al., 2014; Wertz et al., 1989), covers the whole cell surface in the stratum corneum and is believed to act as a template for the orientation of the free barrier lipids and prevent permeable boundaries between the lipids and cells (Behne et al., 2000). Any major defects in the biosynthesis or transport of lipids of the corneocyte lipid envelope are lethal (Jennemann et al., 2012; Vasireddy et al., 2007).

MOLECULAR ARRANGEMENT OF THE SKIN LIPID BARRIER

The molecular arrangement of the stratum corneum lipids is also highly specialized: the skin barrier lipids do not form conventional bilayers but multilamellar membranes with the

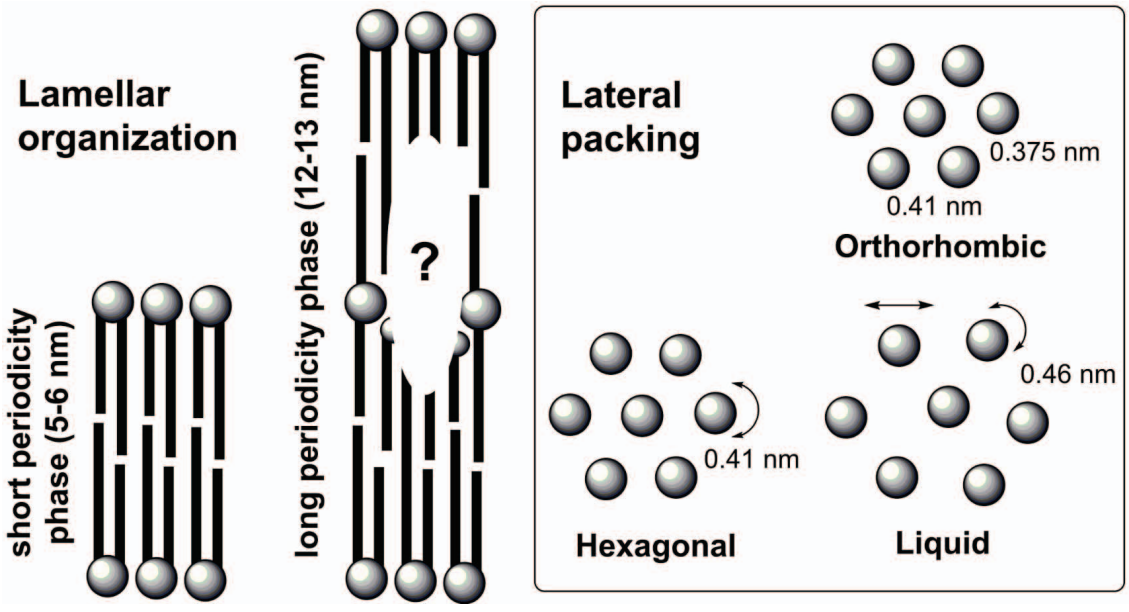

Figure 3. Lamellar and lateral organization of the stratum corneum lipid membranes.

first lipid layer covalently anchored to the corneocyte surface (Breathnach, 1975; Grayson and Elias, 1982). In contrast to phospholipids, the stratum corneum ceramides have a small polar head and very long, saturated chains with prevailing *all-trans* conformation. The prevalent lateral packing of the skin barrier lipids is orthorhombic, which is a very tight packing with highly limited motional freedom. In addition, some lipids are arranged in a hexagonal subcell with greater rotational freedom, and a minor lipid fraction is liquid (**Fig. 3**) (Bouwstra et al., 2001; Damien and Boncheva, 2010; Mendelsohn et al., 2006; Mendelsohn and Moore, 2000; Stahlberg et al., 2015).

Considering the lamellar arrangement of the stratum corneum lipid multilayers, their unique feature is the formation of the so-called long periodicity lamellar phase with a repeat distance of 11.9–13.1 nm (Hou et al., 1991; Madison et al., 1987; Mojumdar et al., 2015a; Neto et al., 2011; White et al., 1988) (**Fig. 3**). This lamellar phase was first observed by electron microscopy and later confirmed by X-ray diffraction. In addition, most studies also describe the presence of a short periodicity phase (with repeat distance of 5.3–6.4 nm) (Bouwstra et al., 1995; Bouwstra et al., 1991; de Jager et al., 2004; de Sousa Neto et al., 2011; Mojumdar et al., 2014; White et al., 1988) and phase separated cholesterol (Craven, 1979; Shieh et al., 1981). Nevertheless, recent experiments on native skin barrier using very high resolution cryo-electron microscopy only detected the long periodicity phase, with the repeat distance of approximately 11 nm (Iwai et al., 2012). There is a consensus that acylceramides (that is, ceramides of the EO-subclass) are necessary for the formation of the long periodicity phase (Bouwstra et al., 1991; de Sousa Neto et al., 2011; Kessner et al., 2010; Madison et al., 1987; Mojumdar et al., 2015a; White et al., 1988). However, recent X-ray diffraction study showed a lamellar phase with 10.6 nm periodicity in ceramide NH membranes without any acylceramide present (Kovacik et al., 2016).

Because of the multilamellar arrangement of lipids in the stratum corneum, both hairpin conformation (with both chains pointing to the same direction) and extended conformation of ceramide (or splayed-chain conformation, with the chains pointing into opposite directions) are theoretically possible (**Fig. 4**). Although the extended conformation is not common in biological membranes, it could be advantageous for the stratum corneum barrier properties (Corkery, 2002; Iwai et al., 2012). First, it would reduce the packing strain of ceramide because they have a smaller cross-section of the polar head than of the chains and there are no lipids with bulky polar heads to compensate for such unfavourable packing ratio of hairpin ceramide. Second, the extended conformation would connect the adjacent lipid lamellae and prevent permeable boundaries.

STRATUM CORNEUM LIPID MEMBRANE MODELS

The exact lipid organization in the stratum corneum has been under debate for decades (Norlen, 2013). Both lamellar phases and the lateral packing can be reproduced using the in vitro lipid membrane models (Kessner et al., 2008). Numerous previous studies using either lipid membrane models or stratum corneum described how ceramide structure influences their behaviour in membranes and permeability (Janusova et al., 2011; Novotný et al., 2009; Pullmannová et al., 2014; Rerek et al., 2001; Skolova et al., 2014; Skolova et al., 2016; Skolova et al., 2013; Stahlberg et al., 2016; Stahlberg et al., 2015) and proposed models of the arrangement (Bouwstra

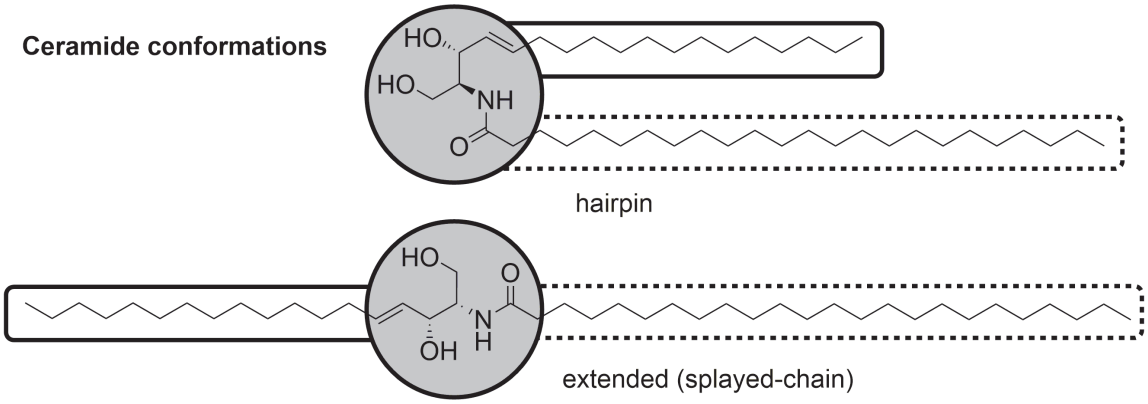

Figure 4. Two possible conformations of ceramide in the skin barrier membranes.

et al., 1991; de Jager et al., 2004; de Sousa Neto et al., 2011; Iwai et al., 2012; Mojumdar et al., 2015a; Mojumdar et al., 2015b; Mojumdar et al., 2014). However, no broad consensus has been reached, mainly because of the differences in the experimental setup, method used and, in case of models, lipid composition.

These lipid models always bear a certain level of simplification but some of them showed very good correlations with real skin properties. For example, de Jager *et al*. studied a model lipid membrane composed of ceramides EOS, NS24, NP24, AS24, NP16, AP24, free fatty acid mixture and cholesterol and found similar permeabilities of this model and isolated stratum corneum to *p*-aminobenzoic acid and its esters (de Jager et al., 2006). We compared the effects of ceramide with shortened chains (both acyl and sphingosine) in skin and simple lipid membranes composed of ceramide NS24, lignoceric acid, cholesterol and cholesteryl sulphate and found similar trends in permeabilities to the two model permeants theophylline and indomethacin (Janůšová et al., 2011; Školová et al., 2016; Školová et al., 2013). Furthermore, a lipid model composed of ceramide NS24, free fatty acids and cholesterol (with or without cholesteryl sulphate) confirmed the existence of fully extended ceramide with cholesterol molecules associated with the ceramide sphingoid moiety and free fatty acids with the acyl chains (Školová et al., 2014) suggested by very high resolution cryo-electron microscopy of native skin (Iwai et al., 2012). The permeabilities of our recent complex model with ceramides EOS, EOdS and EOP, NS, NdS, NP, AS, AdS and AP, free fatty acids, cholesterol and cholesteryl sulphate (the flux values of theophylline and indomethacin were 0.24 ± 0.02 μg/cm^2/h and 0.12 ± 0.02 μg/cm^2/h,(Opálka et al., 2016)) are in very good agreement with those of a membrane model constructed from isolated human skin ceramides (the flux values of theophylline and indomethacin were 0.40 ± 0.05 μg/cm^2/h and 0.23 ± 0.02 μg/cm^2/h, respectively (Pullmannová et al., 2014)) and also with permeabilities of isolated human epidermis under the same conditions (the flux values of theophylline and indomethacin were 0.15 ± 0.05 μg/cm^2/h and 0.05 ± 0.02 μg/cm^2/h, respectively – Kováčik, unpublished data).

The main drawback of the model lipid membranes is that some ceramides are not commercially available, especially those of the EO-subclass and H-subclass. However, synthetic procedures to these lipids have recently been published (Kovacik et al., 2016; Mori and Matsuda, 1991; Muller and Schmidt, 2000; Opálka et al., 2015) and opened the possibility to further improve the stratum corneum lipid models to better mimic the real skin lipid barrier.

CONCLUSION

Ceramides are essential for our life on dry land. Major disturbances to their biosynthesis or transport could be lethal because of an extensive water loss. Even less pronounced alterations of the stratum corneum lipid composition and organization are associated with skin diseases such as atopic dermatitis, psoriasis and ichthyoses and could greatly affect the quality of life of the patients. Although topical application of skin-identical lipids or their analogues has a strong potential to repair the skin barrier in such diseases and prevent inflammation, deeper understanding of the physical chemistry of ceramides and the molecular arrangement of the skin lipid membranes is necessary for more rational design of such therapies.

ACKNOWLEDGEMENTS

This work was supported by the Czech Science Foundation-German Science Foundation joint project 16-2568J.

References

[1] Banks-Schlegel S, Green H. Involucrin synthesis and tissue assembly by keratinocytes in natural and cultured human epithelia. J Cell Biol. 1981;90:732-737.
[2] Behne M, Uchida Y, Seki T, de Montellano PO, Elias PM, Holleran WM. J. Invest. Dermatol. 2000;114:185.
[3] Bouwstra JA, Gooris GS, Bras W, Downing DT. Lipid organization in pig stratum corneum. J. Lipid. Res. 1995;36:685-695.
[4] Bouwstra JA, Gooris GS, Dubbelaar FE, Ponec M. Phase behavior of lipid mixtures based on human ceramides: coexistence of crystalline and liquid phases. J. Lipid. Res. 2001;42:1759-1770.
[5] Bouwstra JA, Gooris GS, van der Spek JA, Bras W. Structural investigations of human stratum corneum by small-angle X-ray scattering. J. Invest. Dermatol. 1991;97:1005-1012.
[6] Bouwstra JA, Ponec M. The skin barrier in healthy and diseased state. Biochim. Biophys. Acta. 2006;1758:2080-2095.
[7] Breathnach AS. Aspects of epidermal ultrastructure. J. Invest. Dermatol. 1975;65:2-15.
[8] Breiden B, Sandhoff K. The role of sphingolipid metabolism in cutaneous permeabilitybarrier formation. Biochim Biophys Acta. 2014;1841:441-452.
[9] Candi E, Schmidt R, Melino G. The cornified envelope: a model of cell death in the skin. Nat. Rev. Mol. Cell Biol. 2005;6:328-340.
[10] Corkery RW. The anti-parallel, extended or splayed-chain conformation of amphiphilic lipids. Colloids Surf B Biointerfaces. 2002;26:3-20.
[11] Craven B. Pseudosymmetry in cholesterol monohydrate. Acta Crystallogr Sect B. 1979;35:1123-1128.
[12] Damien F, Boncheva M. The extent of orthorhombic lipid phases in the stratum corneum determines the barrier efficiency of human skin in vivo. J. Invest. Dermatol. 2010;130:611-614.
[13] de Jager M, Gooris G, Ponec M, Bouwstra J. Acylceramide head group architecture affects lipid organization in synthetic ceramide mixtures. J. Invest. Dermatol. 2004;123:911-916.
[14] de Jager M, Groenink W, i Guivernau RB, et al. A novel in vitro percutaneous penetration model: evaluation of barrier properties with p-aminobenzoic acid and two of its derivatives. Pharmaceut.Res. 2006;23:951-960.
[15] de Sousa Neto D, Gooris G, Bouwstra J. Effect of the omega-acylceramides on the lipid organization of stratum corneum model membranes evaluated by X-ray diffraction and FTIR studies (Part I). Chem Phys Lipids. 2011;164:184-195.
[16] Elias PM. Skin barrier function. Curr. Allergy Asthma Rep. 2008;8:299-305.
[17] Elias PM, Goerke J, Friend DS. Mammalian Epidermal Barrier Layer Lipids: Composition and Influence on Structure. J. Invest. Dermatol. 1977;69:535-546.
[18] Elias PM, Gruber R, Crumrine D, et al. Formation and functions of the corneocyte lipid envelope (CLE). Biochim Biophys Acta. 2014;1841:314-318.
[19] Feingold KR, Elias PM. Role of lipids in the formation and maintenance of the cutaneous permeability barrier. Biochim. Biophys. Acta. 2014;1841:280-294.
[20] Grayson S, Elias PM. Isolation and Lipid Biochemical Characterization of Stratum Corneum Membrane Complexes: Implications for the Cutaneous Permeability Barrier. J. Invest. Dermatol. 1982;78:128-135.
[21] Hannun YA. Functions of ceramide in coordinating cellular responses to stress. Science. 1996;274:1855-1859.
[22] Hannun YA, Obeid LM. Principles of bioactive lipid signalling: lessons from sphingolipids. Nat. Rev. Mol. Cell Biol. 2008;9:139-150.
[23] Holleran WM, Takagi Y, Uchida Y. Epidermal sphingolipids: metabolism, function, and roles in skin disorders. FEBS Lett. 2006;580:5456-5466.
[24] Hou SY, Mitra AK, White SH, Menon GK, Ghadially R, Elias PM. Membrane structures in normal and essential fatty acid-deficient stratum corneum: characterization by ruthenium tetroxide staining and x-ray diffraction. J. Invest. Dermatol. 1991;96:215-223.
[25] Iwai I, Han H, den Hollander L, et al. The human skin barrier is organized as stacked bilayers of fully extended ceramides with cholesterol molecules associated with the ceramide sphingoid moiety. J. Invest. Dermatol. 2012;132:2215-2225.
[26] Jakasa I, Koster ES, Calkoen F, et al. Skin barrier function in healthy subjects and patients with atopic dermatitis in relation to filaggrin loss-of-function mutations. J. Invest. Dermatol. 2011;131:540-542.
[27] Janusova B, Zbytovska J, Lorenc P, et al. Effect of ceramide acyl chain length on skin permeability and thermotropic phase behavior of model stratum corneum lipid membranes. Biochim Biophys Acta. 2011;1811:129-137.
[28] Janůšová B, Zbytovská J, Lorenc P, et al. Effect of ceramide acyl chain length on skin permeability and thermotropic phase behavior of model stratum corneum lipid membranes. BBA-Mol. Cell Biol. L. 2011;1811:129-137.
[29] Jennemann R, Rabionet M, Gorgas K, et al. Loss of ceramide synthase 3 causes lethal skin barrier disruption. Hum Mol Genet. 2012;21:586-608.
[30] Jensen JM, Schutze S, Forl M, Kronke M, Proksch E. Roles for tumor necrosis factor receptor p55 and sphingomyelinase in repairing the cutaneous permeability barrier. J. Clin. Invest. 1999;104:1761-1770.
[31] Jungersted JM, Scheer H, Mempel M, et al. Stratum corneum lipids, skin barrier function and filaggrin mutations in patients with atopic eczema. Allergy. 2010;65:911-918.
[32] Kessner D, Brezesinski G, Funari SS, Dobner B, Neubert RH. Impact of the long chain omega-acylceramides on the stratum corneum lipid nanostructure. Part 1: Thermotropic phase behaviour of CER[EOS] and CER[EOP] studied using X-ray powder diffraction and FT-Raman spectroscopy. Chem Phys Lipids. 2010;163:42-50.
[33] Kessner D, Ruettinger A, Kiselev MA, Wartewig S, Neubert RH. Properties of ceramides and their impact on the stratum corneum structure. Part 2: stratum corneum lipid model systems. Skin Pharmacol. Physiol. 2008;21:58-74.
[34] Kovacik A, Opalka L, Silarova M, Roh J, Vavrova K. Synthesis of 6-hydroxyceramide using ruthenium-catalyzed hydrosilylation--protodesilylation. Unexpected formation of a long periodicity lamellar phase in skin lipid membranes. RSC Adv. 2016;6:73343-73350.

[35] Kováčik A, Roh J, Vávrová K. The chemistry and biology of 6 hydroxyceramide, the youngest member of the human sphingolipid family. ChemBioChem. 2014;15:1555–1562.

[36] Lampe MA, Burlingame A, Whitney J, et al. Human stratum corneum lipids: characterization and regional variations. J.Lipid Res. 1983;24:120-130.

[37] Long SA, Wertz PW, Strauss JS, Downing DT. Human stratum corneum polar lipids and desquamation. Arch Dermatol Res. 1985;277:284-287.

[38] Madison KC, Swartzendruber DC, Wertz PW, Downing DT. Presence of intact intercellular lipid lamellae in the upper layers of the stratum corneum. J. Invest. Dermatol. 1987;88:714-718.

[39] Masukawa Y, Narita H, Shimizu E, et al. Characterization of overall ceramide species in human stratum corneum. J. Lipid. Res. 2008;49:1466-1476.

[40] Mendelsohn R, Flach CR, Moore DJ. Determination of molecular conformation and permeation in skin via IR spectroscopy, microscopy, and imaging. Biochim Biophys Acta. 2006;1758:923-933.

[41] Mendelsohn R, Moore DJ. Infrared determination of conformational order and phase behavior in ceramides and stratum corneum models. Methods Enzymol. 2000;312:228-247.

[42] Mizutani Y, Mitsutake S, Tsuji K, Kihara A, Igarashi Y. Ceramide biosynthesis in keratinocyte and its role in skin function. Biochimie. 2009;91:784-790.

[43] Mojumdar EH, Gooris GS, Barlow DJ, Lawrence MJ, Deme B, Bouwstra JA. Skin lipids: localization of ceramide and fatty acid in the unit cell of the long periodicity phase. Biophys J. 2015a;108:2670-2679.

[44] Mojumdar EH, Gooris GS, Bouwstra J. Phase behavior of skin lipid mixtures: the effect of cholesterol on lipid organization. Soft matter. 2015b;11:4326-4336.

[45] Mojumdar EH, Kariman Z, van Kerckhove L, Gooris GS, Bouwstra JA. The role of ceramide chain length distribution on the barrier properties of the skin lipid membranes. Biochim Biophys Acta. 2014;1838:2473-2483.

[46] Mori K, Matsuda H. Syntheisi of sphingosine relatives .10. Synthesis of (2S,3R,4E)-1-O-(beta-D-glucopyranosyl)-N- 30′-(linoleoyloxy)triacontanoyl-4-icosasphingenine, a new esterified cerebroside isolated from human and pig epidermis. Liebigs Ann. Chem. 1991:529-535.

[47] Motta S, Monti M, Sesana S, Caputo R, Carelli S, Ghidoni R. Ceramide composition of the psoriatic scale. Biochim Biophys Acta. 1993;1182:147-151.

[48] Muller S, Schmidt RR. Synthesis of two unique compounds, a ceramide and a cerebroside, occurring in human stratum corneum. J. Prakt. Chem. 2000;342:779-784.

[49] Neto DD, Gooris G, Bouwstra J. Effect of the omega-acylceramides on the lipid organization of stratum corneum model membranes evaluated by X-ray diffraction and FTIR studies (Part I). Chem. Phys. Lipids. 2011;164:184-195.

[50] Norlen L. Current understanding of skin barrier morphology. Skin Pharmacol Physiol. 2013;26:213-216.

[51] Norlen L, Nicander I, Lundsjo A, Cronholm T, Forslind B. A new HPLC-based method for the quantitative analysis of inner stratum corneum lipids with special reference to the free fatty acid fraction. Arch. Dermatol. Res. 1998;290:508-516.

[52] Novotný J, Hrabálek A, Vávrová K. Synthesis and structure-activity relationships of skin ceramides. Curr Med Chem. 2010;17:2301-2324.

[53] Novotný J, Janůšová B, Novotný M, Hrabálek A, Vávrová K. Short-chain ceramides decrease skin barrier properties. Skin Pharmacol. Physiol. 2009;22:22-30.

[54] Opálka L, Kováčik A, Maixner J, Vávrová K. Omega-O-Acylceramides in Skin Lipid Membranes: Effects of Concentration, Sphingoid Base, and Model Complexity on Microstructure and Permeability. Langmuir. 2016;32:12894-12904.

[55] Opálka L, Kováčik A, Sochorová M, et al. Scalable Synthesis of Human Ultralong Chain Ceramides. Org. Lett. 2015;17:5456-5459.

[56] Pullmannová P, Staňková K, Pospíšilová M, Školová B, Zbytovská J, Vávrová K. Effects of sphingomyelin/ceramide ratio on the permeability and microstructure of model stratum corneum lipid membranes. BBA-Biomembranes. 2014;1838:2115-2126.

[57] Rabionet M, Bayerle A, Marsching C, et al. 1-O-acylceramides are natural components of human and mouse epidermis. J. Lipid. Res. 2013;54:3312-3321.

[58] Rabionet M, Gorgas K, Sandhoff R. Ceramide synthesis in the epidermis. Biochim Biophys Acta. 2014;1841:422-434.

[59] Rerek ME, Chen H, Markovic B, et al. Phytosphingosine and Sphingosine Ceramide Headgroup Hydrogen Bonding: Structural Insights through Thermotropic Hydrogen/Deuterium Exchange. J. Phys. Chem. B. 2001;105:9355 -9362.

[60] Robson KJ, Stewart ME, Michelsen S, Lazo ND, Downing DT. 6-Hydroxy-4-sphingenine in human epidermal ceramides. J. Lipid. Res. 1994;35:2060-2068.

[61] Shieh H-S, Hoard LG, Nordman CE. The structure of cholesterol. Acta Crystallogr Sect B. 1981;37:1538-1543.

[62] Schreiner V, Pfeiffer S, Lanzendörfer G, et al. Barrier characteristics of different human skin types investigated with X-ray diffraction, lipid analysis, and electron microscopy imaging. J. Invest. Dermatol. 2000;114:654-660.

[63] Skolova B, Hudska K, Pullmannova P, et al. Different phase behavior and packing of ceramides with long (C16) and very long (C24) acyls in model membranes: infrared spectroscopy using deuterated lipids. J Phys Chem B. 2014;118:10460-10470.

[64] Skolova B, Janusova B, Vavrova K. Ceramides with a pentadecasphingosine chain and short acyls have strong permeabilization effects on skin and model lipid membranes. Biochim Biophys Acta. 2016;1858:220-232.

[65] Skolova B, Janusova B, Zbytovska J, et al. Ceramides in the skin lipid membranes: length matters. Langmuir. 2013;29:15624-15633.

[66] Stahlberg S, Lange S, Dobner B, Huster D. Probing the Role of Ceramide Headgroup Polarity in Short-Chain Model Skin Barrier Lipid Mixtures by (2)H Solid-State NMR Spectroscopy. Langmuir. 2016;32:2023-2031.

[67] Stahlberg S, Skolova B, Madhu PK, Vogel A, Vavrova K, Huster D. Probing the role of the ceramide acyl chain length and sphingosine unsaturation in model skin barrier lipid mixtures by (2)H solid-state NMR spectroscopy. Langmuir. 2015;31:4906-4915.

[68] Školová B, Hudská Kr, Pullmannová P, et al. Different phase behavior and packing of ceramides with long (C16) and very long (C24) acyls in model membranes: infrared spectroscopy using deuterated lipids. J. Phys. Chem. B. 2014;118:10460-10470.

[69] Školová B, Janůšová B, Vávrová K. Ceramides with a pentadecasphingosine chain and short acyls have strong permeabilization effects on skin and model lipid membranes. BBA-Biomembranes. 2016;1858:220-232.

[70] Školová B, Janůšová B, Zbytovská J, et al. Ceramides in the skin lipid membranes: length matters. Langmuir. 2013;29:15624-15633.

[71] t'Kindt R, Jorge L, Dumont E, et al. Profiling and characterizing skin ceramides using reversed-phase liquid chromatography--quadrupole time-of-flight mass spectrometry. Anal Chem. 2012;84:403-411.

[72] Uchida Y, Holleran WM. Omega-O-acylceramide, a lipid essential for mammalian survival. Journal of Dermatological Science. 2008;51:77-87.

[73] van Smeden J, Boiten WA, Hankemeier T, Rissmann R, Bouwstra JA, Vreeken RJ. Combined LC/MS-platform for analysis of all major stratum corneum lipids, and the profiling of skin substitutes. Biochim Biophys Acta. 2014a;1841:70-79.

[74] van Smeden J, Hoppel L, van der Heijden R, Hankemeier T, Vreeken RJ, Bouwstra JA. LC/MS analysis of stratum corneum lipids: ceramide profiling and discovery. J. Lipid Res. 2011;52:1211-1221.

[75] van Smeden J, Janssens M, Gooris GS, Bouwstra JA. The important role of stratum corneum lipids for the cutaneous barrier function. Biochim Biophys Acta. 2014b;1841:295-313.

[76] Vasireddy V, Uchida Y, Salem N, et al. Hum. Mol. Genet. 2007;16:471.

[77] Vavrova K, Henkes D, Struver K, et al. Filaggrin Deficiency Leads to Impaired Lipid Profile and Altered Acidification Pathways in a 3D Skin Construct. J Invest Dermatol. 2014;134:746-753.

[78] Wertz PW, Madison KC, Downing DT. Covalently bound lipids of human stratum corneum. J. Invest. Dermatol. 1989;92:109-111.

[79] White SH, Mirejovsky D, King GI. Structure of lamellar lipid domains and corneocyte envelopes of murine stratum corneum. An X-ray diffraction study. Biochemistry. 1988;27:3725-3732.